

## Reviewed Preprint

v1 • February 27, 2025

Not revised

## Reviewed Preprint

v2 • April 17, 2026

Revised by authors

## ✉ For correspondence:

[diannahidalgo@g.harvard.edu](mailto:diannahidalgo@g.harvard.edu)[gabriel.kreiman@tch.harvard.edu](mailto:gabriel.kreiman@tch.harvard.edu)

† These authors contributed equally to this work

**Competing interests:** No competing interests declared

**Funding:** See [page 38](#)

**Reviewing editor:** Kristine Krug, Otto-von-Guericke University Magdeburg, Germany

© 2025, Hidalgo et al. This article is distributed under the terms of the [Creative Commons Attribution License](#), which permits unrestricted use and redistribution provided that the original author and source are credited.

# Trial-by-trial inter-areal interactions in visual cortex in the presence or absence of visual stimulation

Dianna Hidalgo<sup>1,†</sup> ✉, Giorgia Dellaferrera<sup>2,†</sup>, Giordano Ramos-Traslosheros<sup>1</sup>, Will Xiao<sup>1</sup>, Carlos R Ponce<sup>1</sup>, Maria Papadopouli<sup>3,4,5</sup>, Stelios Smirnakis<sup>6,7</sup>, Gabriel Kreiman<sup>2</sup> ✉

<sup>1</sup>Department of Neurobiology, Harvard Medical School, Boston, United States • <sup>2</sup>Children's Hospital, Harvard Medical School, Boston, United States • <sup>3</sup>Department of Computer Science, University of Crete, Heraklion, Greece • <sup>4</sup>Institute of Computer Science, FORTH, Heraklion, Greece • <sup>5</sup>Archimedes, Athena R.C., Marousi, Greece • <sup>6</sup>Department of Neurology, Massachusetts General Brigham, Boston, United States • <sup>7</sup>Jamaica Plain Veterans Administration Hospital, Harvard Medical School, Boston, United States

## eLife Assessment

This study investigates trial-by-trial intra- and inter-cortical interactions in the visual cortex of the mouse and the monkey. The authors find that activity in one layer (in mice) or one area (in monkeys) can partially predict neural activity in another layer or area on the single-trial level in different experimental contexts. This **valuable** finding expands previously known contributions of stimulus-independent downstream activity to neural responses in the visual cortex by demonstrating how these change under varying visual stimuli as well as in the absence of visual stimulation. While the methodology is **solid**, the juxtaposition of mouse and monkey data from different modalities and at difference scales limits the interpretability of the observations and forces superficial comparisons. More in-depth focus on either data set in isolation may reveal more nuanced understanding of cortical interactions rather than trying to draw parallels between very different datasets.

<https://doi.org/10.7554/eLife.105119.2.sa4>

## Abstract

State-of-the-art computational models of vision largely focus on fitting trial-averaged spike counts to visual stimuli using overparameterized neural networks. However, a computational model of the visual cortex should predict the dynamic responses of neurons in single trials across different experimental conditions. In this study, we investigated trial-by-trial inter-areal interactions in the visual cortex by predicting neuronal activity in one area based on activity in another, distinguishing between stimulus-driven and non-stimulus-driven shared variability. We analyzed two datasets: calcium imaging from mouse V1 layers 2/3 and 4, and extracellular neurophysiological recordings from macaque V1 and V4. Our results show that neuronal activity can be predicted bidirectionally between L2/3 and L4 in mice, and between V1 and V4 in macaque monkeys, with the latter interaction exhibiting directional asymmetry. The predictability of neuronal responses varied with the type of visual stimulus, yet responses could also be predicted in the absence of visual stimulation. In mice, we observed a bimodal distribution of neurons, with some neurons primarily driven by visual inputs and others showing predictable activity during spontaneous activity despite lacking consistent visually evoked responses. Predictability also depended on intrinsic neuronal properties, receptive field overlap, and the relative timing of activity across areas. Our findings highlight the presence of both stimulus- and non-stimulus-

related components in interactions between visual areas across diverse contexts and underscore the importance of non-visual shared variability between visual regions in both mice and macaques.

## Introduction

To predict the activity of neurons in the visual cortex, multiple studies have focused on correlating external stimuli with trial-averaged responses (Hubel and Wiesel, 1962 [↗](#); Pasupathy et al., 2020 [↗](#)). Between the stimulus and specific cortical neurons, there is a complex signal processing cascade involving multiple processing stages. Therefore, computational models of visual processing typically gloss over most of the relevant biological machinery in an attempt to fit average firing rates from images (Serre et al., 2007 [↗](#)a; Yamins et al., 2014 [↗](#)). A mechanistic understanding of the factors that govern firing in the visual cortex requires models that can capture the trial-by-trial transformations across those processing stages. Moreover, neurons throughout the cortex fire “spontaneously” in the absence of any visual input. Thus, by definition, any model predicting neuronal activity that is exclusively dependent on visual stimulation does not account for such fluctuations. Previous studies in mice have revealed significant non-visual influences in neuronal activity in cortex, even in V1, partly accounted for by movement (Stringer et al., 2019 [↗](#)b; Avitan and Stringer, 2022 [↗](#); Polack et al., 2013 [↗](#); Niell and Stryker, 2010 [↗](#); Dadarlat and Stryker, 2017 [↗](#)). These observations contrast with a recent macaque study which did not find the same motor-related spontaneous activity in either V1, V2, or V3 (Talluri et al., 2023 [↗](#)). Nevertheless, variables that are not related to movement, such as attention, expectation, and arousal, also modulate stimulus- and non-stimulus driven neuronal activity in monkeys (Reynolds and Chelazzi, 2004 [↗](#); Gazzaley et al., 2007 [↗](#); Okazaki et al., 2008 [↗](#); Gilbert and Li, 2013 [↗](#)), potentially adding to the response variability across stimulus repeats and to neuronal activity in the absence of visual stimuli.

Neuronal interactions between visual areas occur in the presence and absence of visual stimuli (Chen et al., 2022 [↗](#); Stringer et al., 2019 [↗](#)b; Wosniack et al., 2021 [↗](#); Ringach, 2009 [↗](#); Avitan and Stringer, 2022 [↗](#)). Therefore, such interactions can and should be studied both as a function of sensory inputs and contextual cues but also in the absence of external stimulation or task demands (Chacron et al., 2003 [↗](#); Hsu et al., 2004 [↗](#); Ringach, 2009 [↗](#)). A paradigmatic example of inter-areal interactions is the series of synaptically-connected laminar (e.g. layer 4 → layer 2/3) and cortical areas (e.g. V1 → V2 → V4 → IT) within the ventral visual stream (Lee et al., 2016 [↗](#); Felleman and Van Essen, 1991 [↗](#); Markov et al., 2014 [↗](#); Douglas and Martin, 2004 [↗](#); Wang and Burkhalter, 2007 [↗](#); The MICrONS Consortium et al., 2021 [↗](#)). Due to feedforward, feedback, and horizontal connections in the ventral visual stream, the inter-areal interactions could represent reliable shared visual and non-visual information. Several studies examined interactions between visual areas in mice and macaques, focusing on the entire population level (Semedo et al., 2019 [↗](#), 2022 [↗](#); Tang et al., 2023 [↗](#); Morales-Gregorio et al., 2024 [↗](#)), trial-averaged responses removing transient fluctuations (Semedo et al., 2019 [↗](#)), neuronal activity in response to only one image presentation (Semedo et al., 2019 [↗](#), 2022 [↗](#)), or in the absence of any stimulus (Morales-Gregorio et al., 2024 [↗](#)). Here we investigated interactions between areas in single trials at the level of cortical layers or brain areas across different stimulus types or in the absence of visual stimulation, across different species, and across different recording techniques and temporal resolutions. Throughout, we use the term “interactions” to denote shared variability at the single-trial level, including stimulus-induced correlations and trial-by-trial stimulus-independent fluctuations which can arise from internal state, contextual inputs, or other top-down factors. We focused on multiple simultaneously recorded areas of the ventral visual stream to assess the stimulus- and non-stimulus-driven variability shared between cortical subnetworks. We found that it is possible to reciprocally predict neuronal activity, both during visual stimulation but also during spontaneous activity, and that this predictability depends on the intrinsic properties of each neuron, the degree of receptive field overlap, and the relative timing of activity across areas.

## Results

### Layer 4 activity predicts layer 2/3 activity and V1 activity predicts V4 activity in single trials

We studied neuronal activity from two open datasets: mouse neurons in V1 layer 4 and layers 2/3 (L4 and L2/3; calcium imaging; Figure 1A) (Stringer et al., 2019a) and macaque monkey multiunit sites in areas V1 and V4 (extracellular electrophysiology; Figure 1B) (Chen et al., 2022). In addition, we recorded new data from an additional monkey during spontaneous activity and using the same visual stimuli as in Chen et al. (2022) (Methods). The mouse neuronal recordings we used for this experiment were based on approx. 5,500 neurons per mouse (n=4, Table 1) responding to visual stimuli (drifting gratings or static natural black and white images; total of 7 recording days), in addition to “spontaneous” activity during approximately 30 minutes of gray/black screen presentation on 6 of the 7 recording days. The monkey recordings were based on a range of 32-803 electrodes per animal (3 monkeys, L, A, and D; Table 2) responding to visual stimuli (full-size static checkerboard image; n=3 recordings for monkey L, n=1 for monkey A, n=2 for monkey D), small and thin bar slow-moving in a small clockwise square direction (n=1 for monkeys L and A); or large and thick bar fast-moving in a big clockwise square direction (n=1 for monkeys L and A) in addition to spontaneous activity during gray screen presentation in all recording days (n=5 for monkey L, n=3 for monkey A, n=2 for monkey D). The recordings consisted of multi-unit activity (MUAe) and local field potentials (LFP) in monkeys L and A retrieved from the open dataset by Chen et al. (Chen et al., 2022). Monkey D recordings were acquired using the same checkerboard stimulus presentation conditions as stated in Chen et al. (2022). There was also a lights-off condition, where the head-fixed monkeys were free to open or close eyes for approximately 10-25 minutes (monkeys L/D; 2-3 recording days). We omitted channels with signal-to-noise ratio of less than 2, or channels that were considered “spurious” by the authors of the open dataset (Chen et al., 2022).

We evaluated two types of interactions between areas: inter-laminar (Figure 1C; mouse V1) and inter-cortical (Figure 1D; monkey). We used linear ridge regression to predict neuronal activity in one area from activity in the other area in single trials (Figure 1E, see Methods) (Semedo et al., 2019). For each neuron/site in the target area we fit a linear readout from the other area’s simultaneous population activity on the same trial, with an  $L_2$  (“ridge”) penalty. Performance was evaluated using cross-validation over trials and quantified as squared Pearson’s  $r$  (hereafter, “explained variance” or EV, Methods). Figure 2A shows sample neuronal activity from three example mouse V1 L2/3 cells during image presentation (black traces). Overlaid, the figure also shows the predicted neuronal activity (red). The predicted neuronal activity is shown as a function of the actual activity in response to every image presentation for the same example cells in Figure 2C. The top cell illustrates a case where the predicted activity closely matches the actual activity ( $EV = 0.67$ ), the middle cell shows a typical case ( $EV = 0.39$ ), and the bottom cell illustrates a case where the predictions deviated from the actual neuronal activity ( $EV = 0.07$ ). We focused on neurons deemed “visually reliable” (~17% of total L2/3 neurons; Table 1, Methods, see results for all neurons in Figure Supplement 1C). The ridge regression model predicted single-trial L2/3 activity from L4 activity across both types of visual stimuli with an average EV of  $0.28 \pm 0.16$  (mean  $\pm$  stdev. across neurons, Figure 2E) whereas the shuffle control mean EV was  $0.004 \pm 0.002$ .

In monkeys, trial-to-trial variations in V4 activity were predicted from V1 activity across the three types of visual stimuli. Example recording sites for monkey L are shown in Figure 2B, D (see also Figure Supplement 1 D-G for examples from two additional monkeys, A and D). The ridge regression model predicted the single-trial responses in V4 activity from V1 activity with an average EV of  $0.30 \pm 0.15$  (Figure 2F for monkey L, see Figure Supplement 1H for monkey A and Figure Supplement 1I for monkey D), whereas the shuffle control mean EV was  $0.005 \pm 0.005$ . Most sites in V4 (72.3%) were deemed visually reliable; EV results for all monkey sites are shown in Figure Supplement 1J. EV performance varied across the three monkeys ( $EV_L = 0.34$ ,  $EV_A = 0.21$ ,  $EV_D = 0.11$ ). This variation may be due to predictor population size (Table 2). We

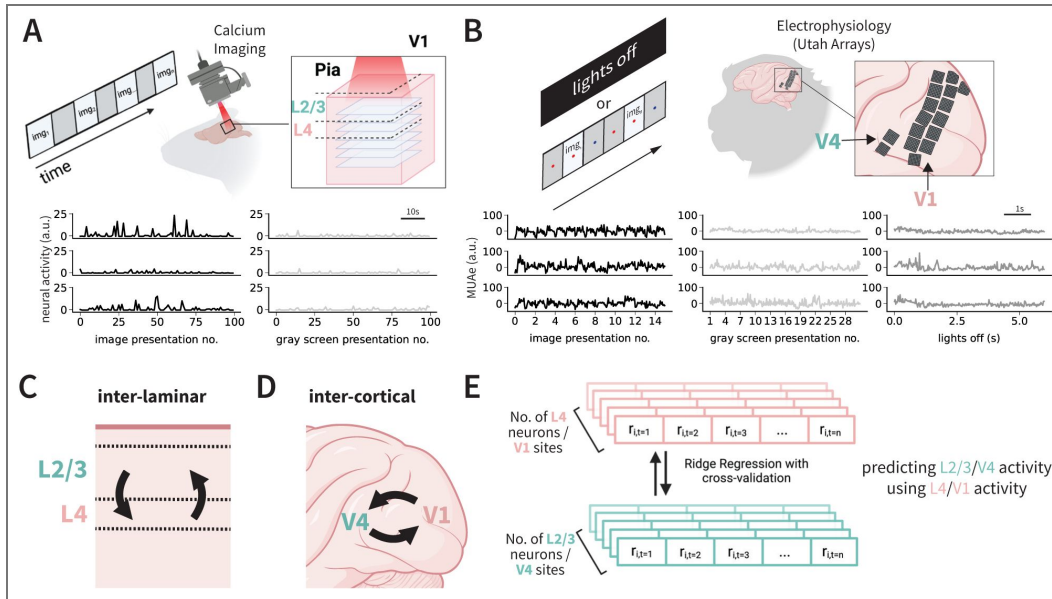


**Figure 1. Predicting trial-to-trial and timepoint-to-timepoint neuronal activity between areas.**

**A.** Top: Experimental set-up to record two-photon Calcium imaging activity data from layers 2/3 (L2/3) and layer 4 (L4) in rodent V1 upon presentation of gratings, natural stimuli or gray screen images (represented as  $img_n$ ) (Stringer et al., 2019a). Deconvolved calcium imaging traces were z-scored using baseline activity during 30 minutes of gray screen presentation before/after image presentation (Table 1). Bottom: Sample z-scored neuronal activity from 3 different neurons in response to 100 presentations of drifting gratings (left) or gray screen presentations (right). Each activity value corresponds to one image presentation, and was calculated as the average of two calcium imaging video frames (666 ms or 800 ms, see details in Methods). **B.** Top: Experimental set-up for the neuronal activity data from monkeys V1 and V4 (Chen et al., 2022). Electrophysiological activity was simultaneously recorded across 1,024 channels from 16 Utah arrays (Table 2). Bottom: Envelope multiunit spiking activity (MUAe) from 3 different sites in response to multiple presentations of a repeated 400 ms full-field checkerboard image (left, baseline mean-subtracted), 200 ms gray screen (middle), or during a lights-off condition (30 minutes total; right). Each value corresponds to aggregated MUAe activity in a 25-ms bin. **C.** Overview of inter-laminar relationships examined in mouse V1. “Lower level” layer 4 (L4) neuronal activity is used to predict “higher level” layer 2/3 (L2/3) activity and vice versa. **D.** Overview of inter-cortical relationships examined in monkeys, where lower-level V1 is used to predict higher-level V4 (blue arrow) and vice versa (red arrow). **E.** Illustration of linear ridge regression method used for inter-areal prediction. Neuronal activity in response to presentation number  $i$  (labeled “ $r_i$ ”) at time  $t$  from one area (e.g., mouse V1 L2/3 or monkey V1) was used to predict activity in the other area (e.g., mouse V1 L4 or monkey V4) (Semedo et al., 2019). Predictability was evaluated using 10-fold cross-validation across presentation trials in mice, and across 25-ms timepoints in monkeys (Methods).

**Table 1. Mouse neuron counts used for inter-layer prediction and analyses.**

A total of 7 recordings were used to perform prediction experiments. Each row corresponds to a recording day, containing the dataset recording type (Mouse Dataset), total number of neurons, and visually reliable neurons (see Methods). Fourth column: In the directionality prediction experiments, the area containing more neurons (L2/3) was further subsampled to match the number of L4 neurons. The dataset recording type names contain either “ori32” or “nating32”, in addition to the mouse name (MP0-). “nating32” represents the dataset of the 32 natural image presentations. “ori32” represents the dataset of the 32 drifting gratings.

Mouse Dataset	Layer 2/3			Layer 4	
	Total	visually reliable	Subsampled (directionality)	Total	visually reliable
nating32 MP031	6615	1248	219	2367	219
nating32 MP032	7980	1549	96	1441	96
nating32 MP033	6646	1467	164	2010	164
ori32 MP027	6264	1029	211	2346	211
ori32 MP031	5423	455	78	1382	78
ori32 MP032	5420	274	47	923	47
ori32 MP033	5277	1243	298	1588	298
Total	43625	7265	1113	12057	1113

**Table 2. Monkey site counts used for intercortical prediction and analyses.**

First column: First letter denotes the monkey name, followed by the date, followed by the dataset type acquired during the session (C: Checkerboard presentations, G: Gray screen, L: Lights-off condition, LB: Large, thick moving bars, SB: Small, thin moving bars). Fourth column: In the directionality prediction experiments, the area containing more sites was further subsampled to match the number of V4 sites.

Monkey Datasets	V1			V4	
	Total	visually reliable	Subsampled (directionality)	Total	visually reliable
L 090817 (C,G,L)	627	555	73	96	73
L 100817 (C,G,L)	688	587	83	115	83
L 250717 (C,G,L)	645	537	72	86	72
L 260617 (LB,G)	645	592	82	86	82
L 280617 (SB,G)	645	518	68	86	68
A 041018 (C,G)	571	357	44	76	44
A 280818 (LB,G)	571	381	58	76	58
A 290818 (SB,G)	571	251	30	76	30
D 250225 (C,G,L)	16	8	-	16	7
D 260225 (C,G,L)	16	10	-	16	10
Total	4995	3796	510	729	527

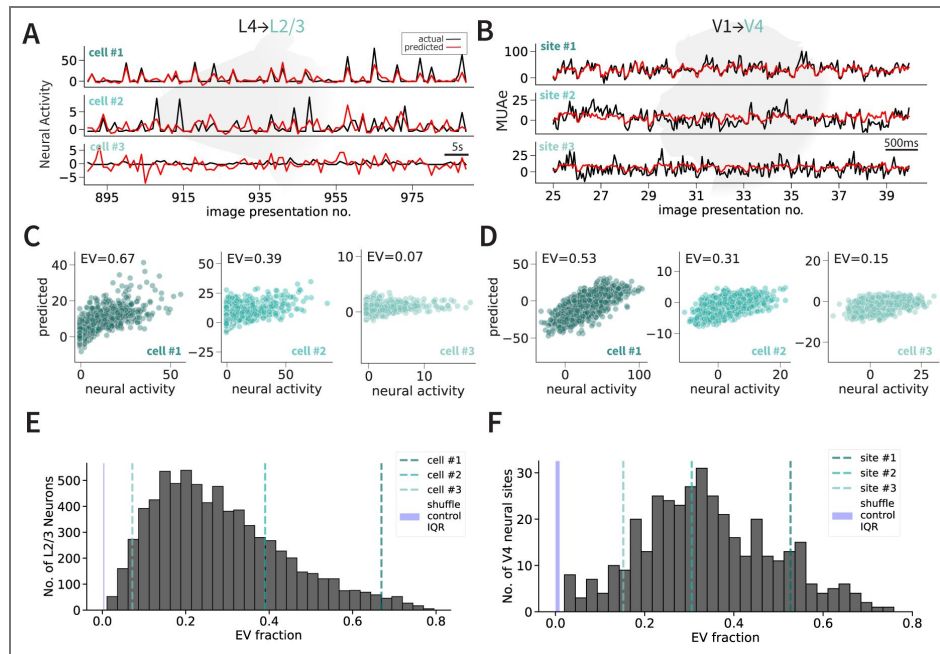


**Figure 2. Lower level activity can predict higher level activity in both rodent and primate brains.**

**A.** Example neuronal activity (z-scored, black) in response to stimulus presentations (drifting gratings) in mouse V1 L2/3 along with regression-model predictions (red) for a typical cell (2, middle), cell in the top 10% percentile of predictability (1, top), and bottom 10% percentile (3, bottom). **B.** Same as A for monkey MUAe activity in response to a full-field checkerboard image in three V4 neuronal sites. **C.** Predicted neuronal activity versus actual neuronal activity in response to stimuli for the mouse L2/3 cells 1, 2, and 3 shown in A. Each point represents 800 ms, corresponding to a stimulus presentation.  $r$  values (top left) indicate the correlation coefficient. **D.** Same as C for monkey V4 neuronal sites 1, 2, and 3. Each point represents one 25-ms timepoint during the 400-ms presentation. **E.** Distribution of EV fraction in L4 → L2/3 regressions of neural activity in response to visual stimuli in cells that were deemed visually reliable in 4 mice and 7 recording days ( $n = 7$ , 265 neurons, Methods). Performance using 10-fold cross-validation across trials was quantified as squared Pearson's  $r$ , referred to as explained variance (EV) fraction. The three vertical lines show the 3 examples in part A, C. The blue solid shaded rectangle (here and throughout) represents the interquartile range (IQR) shuffle control performance, where the activity timepoints of one area were randomly shuffled. **F.** Distribution of EV fraction in V1 → V4 regressions of neural activity in response to visual stimuli in sites deemed visually reliable in monkey L (5 recording days, 68–82 V4 sites recorded per day;  $n = 378$  total site recordings).

subsampling sites in monkey L to match the numbers of monkey A and monkey D (20 permutations; [Figure Supplement 1L](#)); subsampling was performed for all analyses hereafter unless noted). Subsampling monkey L matching the number of sites in monkey A (monkey  $L_A$ ) showed an average EV of  $0.35 \pm 0.14$ , statistically higher compared to the EV for monkey A ( $p < 0.001$ , permutation test). Similarly, subsampling monkey L matching the number of sites in monkey D (monkey  $L_D$ ) showed an average EV of  $0.19 \pm 0.11$ , statistically higher compared to the EV for monkey D ( $p < 0.001$ , permutation test).

We asked whether the conclusions were dependent on the model and parameter choices. As an alternative approach to ridge regression, we also fit a Poisson general linear model (GLM) enforcing non-negativity to monkey MUAe without baseline subtraction, using identical folds, bin widths, and temporal gaps as in the ridge regression analysis. The results from the Poisson GLM were consistent with the results obtained using ridge regression ([Figure Supplement 1M](#)). Additionally, to evaluate the impact of the bin size on the results, we re-estimated EV after binning MUAe into 10–200 ms. EV increased with bin size and remained well above shuffle controls across conditions ([Figure Supplement 4A–C](#),  $p < 0.001$ , paired permutation test), indicating that inter-areal predictability is robust across a broad range of physiologically relevant timescales.

In sum, it was possible to provide estimates of neuronal activity in single trials in both species, across different layers within primary visual cortex in mice and across different visual cortical areas in monkeys.

## Inter-cortical predictions are asymmetrical

In the previous section, we demonstrated the possibility of predicting L2/3 activity from L4 activity and V4 from V1. We asked whether we could also predict neuronal responses in the opposite direction. We could predict L4 activity from L2/3 activity in mice and V1 activity from V4 activity in monkeys ([Figure Supplement 1A](#) for mice, [Figure Supplement 1K](#) for monkeys). To directly compare predictability between directions in mice and monkeys, we matched the number of predictors (i.e., number of neurons/sites used to predict activity) and the degree of self-consistency (split-half  $r$  values) by randomly subsampling in each layer or cortical region prior to computing the predictability metrics ([Figure 3A, C](#), Methods).

In mice, there was no statistically significant difference between L4 → L2/3 and L2/3 → L4 directions ( $p > 0.05$ , hierarchical permutation test, [Figure 3B](#)). In monkeys, after matching predictor count and split-half correlation values, the EV fraction in the V1 → V4 direction was higher than in the V4 → V1 direction ( $p < 0.001$  for monkey L, [Figure 3D](#);  $p < 0.05$  for monkey A, [Figure Supplement 3C](#)). This directional asymmetry was stable across temporal bin sizes in monkey L ([Figure Supplement 4D](#)). In monkey A, the asymmetry was small and was not robust across different bin sizes ([Figure Supplement 4E](#)), consistent with the noisier data and weaker effect size in that animal. There were not enough sites with similar reliability distributions in monkey D to perform the matched subsampling directionality tests.

Although we accounted for predictor size and reliability distributions, differences in prediction performance between directions could still reflect additional inherent differences in target-population properties ([Figure Supplement 2F–J](#)). To control for these differences, we modeled EV as a function of target-population properties and used the residuals for inference,  $EV_{\text{resid}} = EV - \hat{E}V$ . Covariates included self-consistency, SNR, one-vs-rest  $r^2$ , and variance metrics (Methods). After adjustment, the difference between inter-cortical directions remained statistically significant overall ( $p < 0.001$  for monkey L,  $p < 0.001$  for monkey A, [Figure Supplement 3F–G](#)). These results suggest that the differences between directions cannot be attributed to target-related neuronal properties. We also analyzed the residuals in mice prediction directions, and after controlling for neuron properties, we still found no statistically significant difference in predictability directions ([Figure Supplement 3E](#),  $p = 0.22$  for stimulus activity,  $p = 0.48$  for gray screen activity).

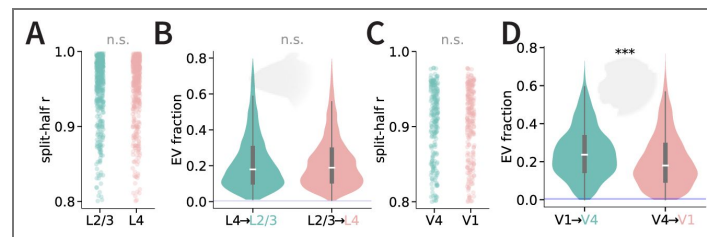


**Figure 3. Asymmetry in inter-cortical predictability in monkeys but not inter-laminar predictability in mice.**

**A.** Split-half reliability (Methods) for the  $n = 298$  neurons (per area) in mouse MP033 drifting gratings presentation recording of V1 L2/3 (green) and L4 (coral) used to perform directionality comparisons. Neurons were randomly subsampled to match the numbers and self-reliability in the two distributions. Here and throughout, asterisks indicate statistically significant differences using a hierarchical independent permutation test (10,000 permutations): \*  $p < 0.05$ , \*\*  $p < 0.01$ , \*\*\*  $p < 0.001$ ; “n.s.” indicates  $p > 0.05$ . **B.** Violin plots describing the distribution of EV fraction for L4  $\rightarrow$  L2/3 (green) and L2/3  $\rightarrow$  L4 (coral) predictions across all 7 stimulus recordings ( $n = 1, 113$  neurons per area). Violin plots (here and throughout) represent the distribution of neuron/site values, with width representing density and inner boxplot representing the interquartile range. Whiskers of each inner box represent the data range. **C.** Example of split-half reliability for the  $n = 74$  sites (per area) in monkey L checkerboard recording (date=090817) of V4 (green) and V1 (coral) used to perform directionality comparisons. **D.** Violin plots describing the distribution of EV fraction for V1  $\rightarrow$  V4 (green) and V4  $\rightarrow$  V1 (coral) across all 5 stimulus recordings ( $n = 786$  sites recordings per area).

## Predictability of neuronal activity is dependent on the visual stimulus

We evaluated whether the predictability of neuronal activity varied with the type of visual stimulus presented to the animal. In mice, we compared the inter-laminar prediction of neuronal activity of visually reliable neurons in response to drifting gratings versus natural images (Figure 4A). We could predict mouse L4 and L2/3 activity under both stimulus conditions ( $p < 0.001$ , paired permutation test of prediction vs. shuffled frames prediction). Predictability was higher for drifting gratings than natural images in the L4 → L2/3 direction (Figure 4B;  $p < 0.001$ , hierarchical permutation test).

In monkeys L and A, we compared inter-cortical predictability of visually reliable sites in responses to a slow-moving small thin bar, fast-moving large thick bar, and a full-size checkerboard image (Figure 4C). As expected, V1 and V4 could predict each other's neural activity across all stimulus types ( $p < 0.001$ , paired permutation test of prediction vs. shuffled frames prediction). The predictability was highest in both directions for neuronal activity in response to a full-field checker-board image (monkey L Figure 4D; monkey A Figure Supplement 5F). In the V1 → V4 direction, the EV fraction was higher when predicting a slow-moving small thin bar compared to a fast-moving large thick bar (monkey L Figure 4D, left; monkey A Figure Supplement 5F, left).

In the V4 → V1 direction, there was no consistency in prediction differences between monkey L and monkey A. In monkey L (V4 → V1), the EV for fast-moving large thick bars was larger than for the slow-moving thin bars ( $p < 0.001$ , permutation test; Figure 4D, right), whereas this difference was flipped in monkey A ( $p < 0.001$ ; Figure Supplement 5F, right). This observation could be due to differences in the degree of reliability in the neuronal responses between monkeys (Figure Supplement 5H, L for monkeys L, A, respectively). We modeled EV as a function of SNR, self-consistency (split-half  $r$ ), variance across time within stimulus, and variance across trials within timepoint, and used  $EV_{\text{resid}} = EV - \hat{EV}$  for inference (Methods). In monkey L (V4 → V1), the difference in EV residuals between thin and thick bars was not statistically significant ( $p = 0.44$ ; Figure Supplement 5K, right), whereas this difference remained statistically significant in monkey A ( $p < 0.001$ ; Figure Supplement 5O, right). Lastly, in the V1 → V4 direction, EV residuals remained statistically higher when predicting the responses to the thin bar compared to the thick bar in both monkeys L and A ( $p < 0.001$  for both monkeys; Figure Supplement 5K, O, left).

## Neuronal activity could be predicted even during spontaneous activity

Given the dependence on the visual stimulus, we next asked whether it would be possible to predict neuronal responses in the absence of any visual stimulus, during “spontaneous activity”. We compared the predictability of stimulus-evoked activity in mice (drifting gratings and natural images) versus the predictability of activity recorded during gray screen presentations. This comparison was conducted in both visually (SNR > 2 & split-half  $r > 0.8$ ) and non-visually (SNR < 2 & split-half  $r < 0.8$ ) reliable neurons ( $n=3$  mice; mouse MP027 did not undergo 30 min. of gray screen presentation). In visually reliable neurons, neuronal activity could still be predicted during the gray screen condition ( $p < 0.001$ , hierarchical paired permutation test compared with shuffled frames). There was a significant reduction in EV during gray screen compared to visual stimulus presentation (Figure 5A left,  $p < 0.001$ , hierarchical paired permutation test). In non-visually reliable neurons, predictability was higher during the gray screen condition compared to stimulus presentation (Figure 5A right,  $p < 0.001$ , hierarchical paired permutation test).

While there was no correlation between neuronal predictability in the responses to visual stimulus presentations and in the response to gray screen presentations in visually reliable neurons (Figure 5B), there was a strong correlation for non-visually reliable neurons (Figure 5C). The difference in predictability in the absence of a stimulus (gray screen presentations) could in principle change according to the directionality in inter-laminar interactions. However, there was

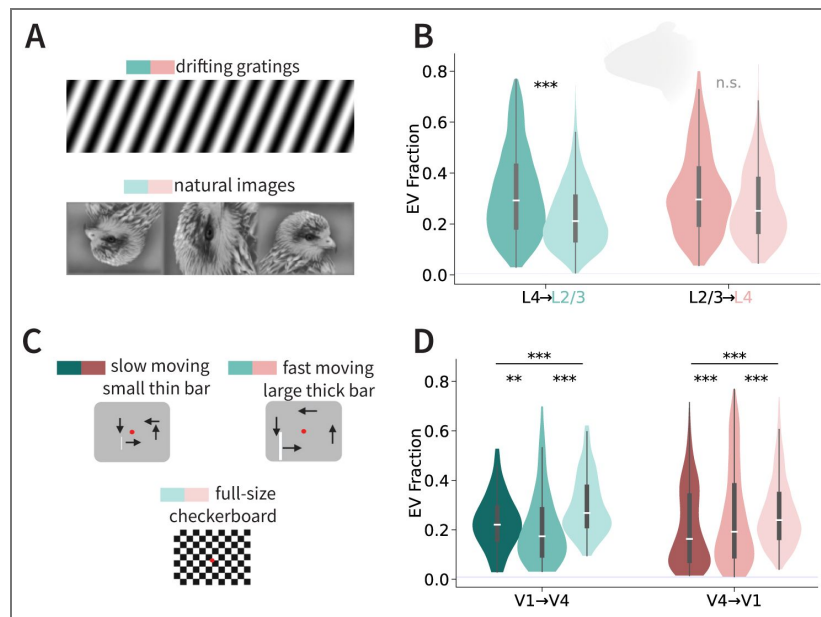


**Figure 4. Stimulus type influences neuronal predictability.**

**A.** Illustration of the two types of stimuli (drifting gratings and static natural images) presented to the mouse during calcium imaging. **B.** Across-layer predictability in mouse V1 for each stimulus type (dark: drifting gratings, light: natural images) and prediction direction. **C.** Illustration of the three types of stimuli presented to the monkeys (Chen et al., 2022). The slow-moving, small, thin bar moved near the fixation point for 1 s in each of the four directions, while the fast-moving, large, thick bar moved towards the edges of the screen for 1 s in each of the four directions. The full-field checkerboard image was presented repeatedly (400 ms each presentation). **D.** Across-area predictability for each stimulus type (dark: slow bars, medium: fast bars, light: checkerboard) and direction.

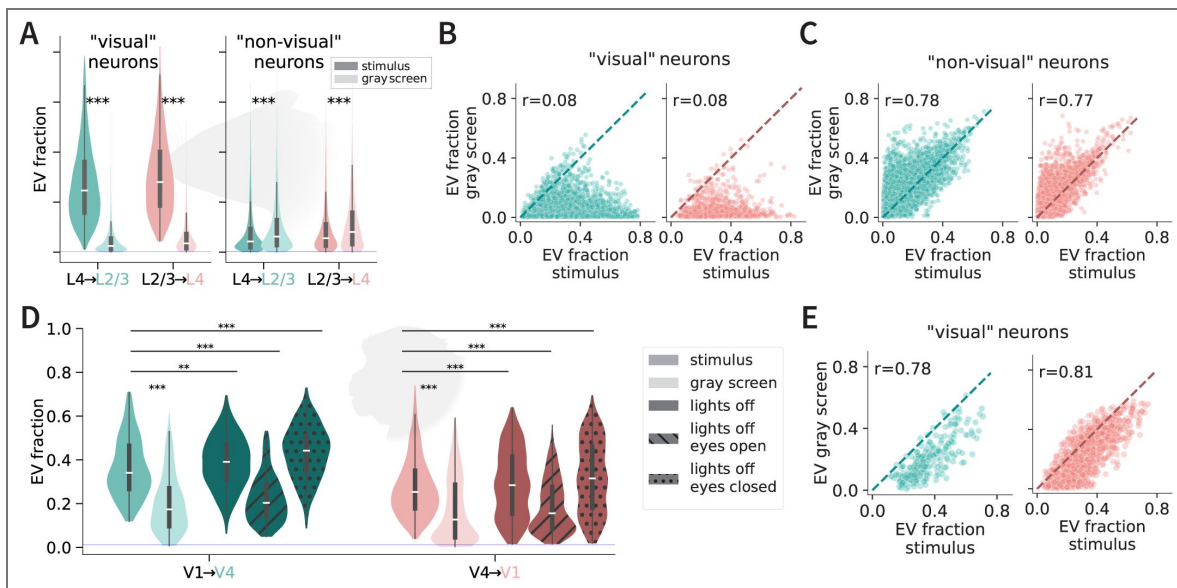


**Figure 5. Spontaneous activity can also be predicted.**

**A.** EV fraction of neuronal activity in response to stimulus presentation (dark violins) or gray screen presentation (light violins) for neurons deemed visually (left) or non-visually (right) reliable (Methods). **B.** Correlation between EV in responses to gray screen (y-axis) versus stimulus presentation (x-axis) in mouse V1 visually reliable neurons (L4 → L2/3:left, green; L2/3 → L4: right, coral). The diagonal line represents the line of equality ( $y=x$ ).  $r$  is the Pearson's  $r$  coefficient. **C.** Same as **B**, but for non-visually reliable neurons. **D.** EV during stimulus presentations (checkerboard image, green), gray screen presentations (light green), or during lights off (dark green). The lights-off condition is further separated into periods when the eyes were open or closed. All lights-off conditions were sub-sampled (10 permutations) to contain similar training lengths as the stimulus and gray screen presentation recordings. **E.** Correlation between EV in responses to gray screen (y-axis) versus stimulus presentation (x-axis) in monkey visually reliable neurons (V1 → V4:left, green; V4 → V1: right, coral). The diagonal line represents the line of equality ( $y=x$ ).  $r$  is the Pearson's  $r$  coefficient. All recorded sites were pulled from the 3 recording days of checkerboard presentations.

no statistically significant difference in the EV fraction between laminar directions (L4 → L2/3 vs. L2/3 → L4), in the same “visually reliable” group and even when subsampling “non-visual” neurons (Figure Supplement 3A [↗](#)).

In monkeys, we only focused on visually reliable sites since the majority of the neuronal population was visually reliable (Figure Supplement 1J [↗](#)). Additionally, an SNR of less than 2 (one of the requirements to define non-visual neurons in the mouse data) most likely reflects artifactual is-sues with the electrode recording the multiunit site (Chen et al., 2022 [↗](#)). We compared inter-areal prediction of stimulus presentation activity (all monkeys for checkerboard presentation; monkeys L and A for moving bars), gray screen presentation (all monkeys), and during lights-off (monkeys L and D). The predictability of neuronal activity in response to gray screen presentation remained statistically above chance ( $p < 0.001$  paired permutation test of prediction vs. shuffled frames pre-diction for all monkeys). The predictability of neuronal activity in the absence of visual stimulus was lower compared to checkerboard presentations (Figure 5D [↗](#),  $p < 0.001$  for monkey L; Figure Supplement 6E [↗](#),  $p < 0.001$  for monkey A; Figure Supplement 6F [↗](#) left,  $p < 0.01$  for monkey D). The same conclusions held when comparing moving bar vs. gray screen presentations (Figure Supplement 6D [↗](#) for monkey L; Figure Supplement 6E [↗](#) for monkey A). Intriguingly, the EV fraction in the lights-off condition was statistically higher than during the stimulus presentations in both directions in monkey L, whereas the EV fraction in the lights-off condition in monkey D was lower (Figure Supplement 6F [↗](#)). Eye closure and sleep can induce global oscillations (Hohaia et al., 2022 [↗](#)) and therefore may lead to correlated neuronal activity, causing an increase in predictability. Mon-key L spent a significant portion with its eyes closed (Chen et al., 2022 [↗](#)), unlike monkey D, who spent almost the entire time with its eyes open (eyes closed duration < 3s in both recording days). To test the effects of eye closure, we further separated the lights-off neuronal activity of into periods where the eyes of monkey L were open or closed. The EV fraction was statistically significantly higher than EV fraction during stimulus presentation activity only during the eyes-closed period (Figure 5D [↗](#)).

The correlation in visual predictability between stimulus presentation and spontaneous activity was high across all types of spontaneous conditions (Figure 5E [↗](#) and Figure Supplement 6C [↗](#) for monkey L; Figure Supplement 6I, J [↗](#) for monkeys A, D, respectively). When assessing the inter-cortical prediction directionality during spontaneous conditions, in monkey L, we found the same asymmetrical relationship as in Figure 3 [↗](#), where V1 → V4 EV fraction was significantly higher than V4 → V1 prediction in both gray screen ( $p < 0.001$ , permutation test) and lights-off ( $p < 0.001$ , permutation test) conditions (Figure Supplement 3B [↗](#)). In monkey A gray screen presentation activity, we did not find any statistically significant difference between direction predictions (Figure Supplement 3C [↗](#), right). However, when accounting for neuronal property differences between the areas, we found the same direction EV asymmetry across both monkeys ( $p < 0.001$ ; Figure Supplement 3F [↗](#) for monkey L; Figure Supplement 3G [↗](#) for monkey A).

## Behavioral metrics account for only a small portion of predictability

Because inter-areal predictability persists in the absence of visual drive, we asked whether behavioral signals could partly account for the inter-laminar and inter-cortical interactions. In mice, augmenting the neural predictability model with face-motion singular value decomposition (SVD) components and running speed did not significantly increase EV relative to the neural-only model in the L2/3 to L4 direction ( $p = 0.77$ , paired permutation test), and had a mild statistical increase in the L4 to L2/3 direction ( $p < 0.05$ , paired permutation test; Figure Supplement 10A [↗](#)). During spontaneous activity, the same type of augmentation did not increase EV relative to the neural-only model in either direction ( $p = 0.095$  for L4 → L2/3 direction,  $p = 0.93$  for L2/3 → L4 direction, paired permutation tests; Figure Supplement 10C [↗](#)). Behavior-only models captured a modest yet statistically significant fraction of variance (stimulus:  $EV = 0.02 \pm 0.03$ , spontaneous:  $EV = 0.01 \pm 0.01$ ;  $p < 0.001$  paired permutation test with shuffled frames). Behavior-only EV correlated with neu-ral EV within areas (stimulus:  $\sim 0.47\text{--}0.50$ ; spontaneous:  $\sim 0.68\text{--}0.69$ ; Figure

Supplement 10B,D [↗](#)), indicating that animals/neurons with stronger neural predictability also tended to show stronger behavior-related structure, but in all cases behavior was not driving the main effect.

In monkey neural recordings during resting state condition (eyes open only), pupil diameter provided a small but significant predictive power ( $EV=0.01 \pm 0.01$ ;  $p < 0.001$  permutation test of prediction vs. shuffled frames prediction). Adding pupil size to the neural model yielded no significant EV gain in either direction ( $p = 1$  in the V1  $\rightarrow$  V4 direction,  $p = 0.70$  in the V4  $\rightarrow$  V1 direction; Figure Supplement 10E [↗](#)).

Together, these results indicate that behavioral metrics contributed a measurable shared component to cross-area predictability, but they are not the principal driver: most explained variance remains tied to the neural population activity.

## Receptive field overlap and neuronal response properties impact predictability

We investigated which neuronal properties are related to the ability to predict responses by comparing EV and key indicators of neuronal response reliability and receptive field properties, in both visually- and non-visually reliable neurons, during either visual presentation or spontaneous conditions. First, we considered the following properties: (i) max  $r^2$  value (i.e., maximum squared correlation between each neuron in the predictor population and the predicted neuron), (ii) 1-vs-rest  $r^2$  self-consistency (squared correlation between each neuron's response to one trial repetition of all stimuli/timepoint with the average response of the rest of the trial repetitions; Methods), (iii) SNR of the predicted neuron, (iv) variance across stimuli, (v) variance across repeats of the same stimulus, (vi) variance across timepoints (monkey data only, since we have multiple timepoints per trial), and (viii) split-half  $r$  (Methods). We plotted EV against each of these variables (mouse: Figure 6B [↗](#); monkey L: Figure 6E [↗](#), monkey A: Figure Supplement 8B [↗](#), monkey D: Figure Supplement 9B [↗](#)) and report the correlation coefficient between EV and each variable in the y-axis in mice (Figure 6A [↗](#)) and monkeys (monkey L: Figure 6D [↗](#), monkey A: Figure Supplement 8A [↗](#), monkey D: Figure Supplement 9A).

In mice, during both stimulus presentation and gray screen presentation, the most correlated property with a neuron's inter-areal predictability was the max  $r^2$  (Figure 6A [↗](#)). For the other 5 properties, there was a strong distinction between stimulus presentation (dark bars) and gray screen presentation (light bars): all 5 properties were positively correlated with the neural activity predictability EV fraction during stimulus presentation, but they were slightly anticorrelated with their predictability EV fraction during gray screen presentation. Because the split-half correlation calculation averages out the non-stimulus-dependent variability in both halves of the trials, it showed a weaker correlation with EV, which depends on trial-by-trial modulation. The one-vs-rest  $r^2$  metric, which also examines trial-by-trial modulation and does not average split-half trials, yielded a stronger correlation with EV during stimulus presentation.

When examining the relationship between 1-vs-rest self-consistency and inter-laminar prediction EV in mice, we observed a bimodal distribution of neurons: one group of neurons showed high EV despite having low self-consistency, and another group showed EV correlated with self-consistency (Figure 6B [↗](#) third column; Figure Supplement 7A [↗](#);  $p < 0.001$ , Hartigan's dip test after thresholding neurons with  $EV > 0.4$ ). The responses of neurons with low self-consistency also showed high EV during gray screen presentation. This bimodality was present in two of the three mice ( $p < 0.001$  for mouse MP031, MP032,  $p = 0.69$  for mouse MP033, Hartigan's dip test; self-consistency and EV fraction relationships across all mice can be seen in Figure Supplement 7B [↗](#)). To better understand the responses of neurons with low self-consistency, we projected out the "non-visual ongoing neuronal activity" from the neuronal responses (Stringer et al., 2019 [↗](#) a) (Methods). This non-visual ongoing activity is deemed to be influenced by spontaneous behavior (Stringer et al., 2019 [↗](#) b). Projecting out this non-visual activity eliminated this bimodality ( $p = 0.71$  and  $p = 0.98$  for L4  $\rightarrow$  L2/3 and L2/3  $\rightarrow$  L4, respectively; Hartigan's dip test, Figure 6C,D [↗](#)). This observation could be because the responses of neurons with low self-consistency can no longer be

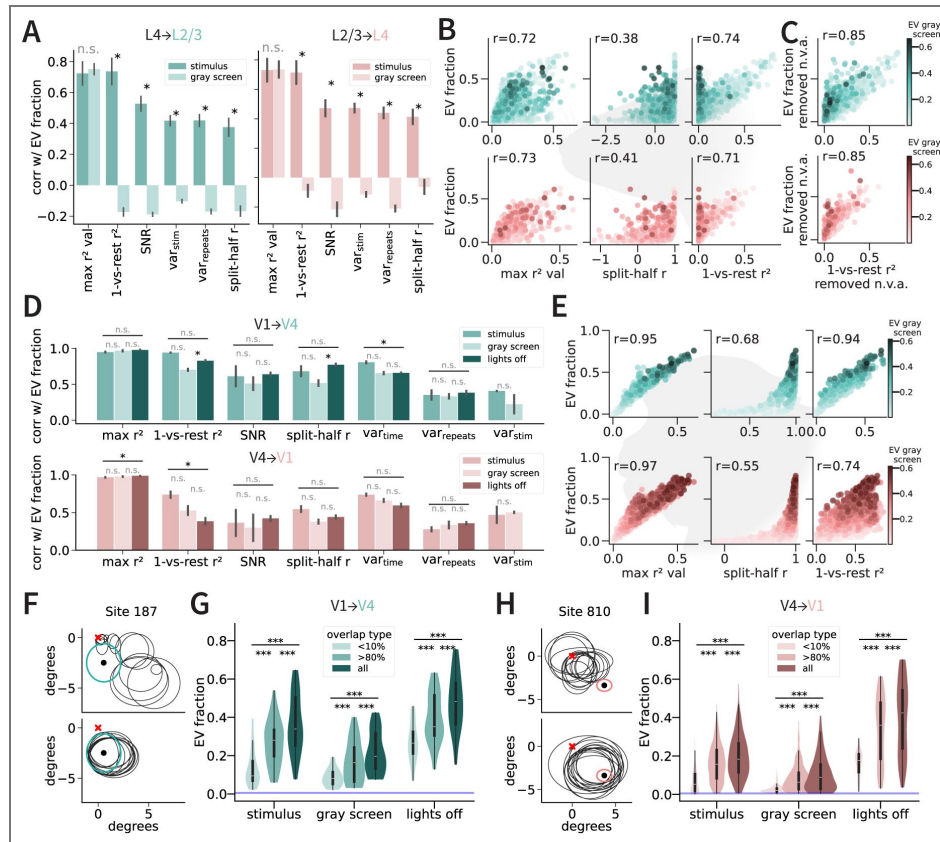


**Figure 6. neuronal predictability depends on SNR, stimulus response variance, and receptive field overlap.**

**A.** Correlation between different neuronal properties with the predictability of L2/3 (green) and L4 (coral) neuronal responses during the presence (dark color) or absence (light color) of visual stimulus. Neuronal properties measured in mouse V1 include the correlation value of the most correlated pair to each cell (max correlation value, squared), a modified metric of self-consistency (one-vs-rest correlation, squared), SNR, variance in the neuronal activity in response to different stimuli, variance in the neuronal activity across repetitions, and the traditional metric of self-consistency (split-half correlation  $r$ ) (Methods). **B.** Relationship between three neuronal properties and their predictability in a randomly chosen sub-sample of neurons ( $n = 4,000$ ) for mouse L2/3 (green) and L4 (coral) neuronal responses from both drifting gratings and natural images conditions (combined). Hue represents the degree of predictability for the same neurons during the 30 minutes of gray screen presentation (see color map on bottom right). **C.** 1-vs-rest squared correlation relationship with predictability after projecting out dimensions of “non-visual” activity (using gray screen activity (Stringer et al., 2019)). **D.** Correlation between different neuronal properties with the predictability of monkey L V4 (green) and V1 (coral) neuronal site recordings during the full-field checkerboard presentation (dark color), gray screen presentation (light color), and lights-off condition (darkest color; solid, hatch lines, and hatch dots). Neuronal properties measured in monkey visual cortex include the max correlation squared value, one-vs-rest squared correlation, SNR, variance across different stimuli (moving bars dataset only), variance across time (within-trial repeat), variance across repeats (within timepoint), and split-half correlation  $r$ . **E.** Same as B for monkey L V1 and V4 neuronal sites. **F.** Top: Receptive fields of one sample V4 neuronal site (green circle, array 2 electrode 187) and 14 randomly selected V1 neuronal sites as predictors (black circles), constrained on sites that share less than 10% receptive field overlap with the V4 site. Bottom: Receptive fields of the same neuronal site 187 and 14 randomly selected V1 neuronal sites used as predictors, constrained on sites that share at least 80% receptive field overlap with the V4 site. **G.** Differences in predictability of V4 neural activity ( $n = 110$  site recordings) in terms of 14 V1 predictor sites with less than 10% RF overlap (light green), 14 predictor sites with at least 80% RF overlap (green), and all predictors (dark green). Predictions were computed for recordings in response to the stimulus presentation (sliding bars and full-field checkerboard images), gray screen presentation, and lights off. **H.** Bottom and top left: Same as F but for monkey L sample V1 site 810. **I.** Same as D, but for V1 ( $n = 970$  site recordings).

predicted, or because the responses of those neurons became more reliable and therefore were highly predicted. To distinguish between these two possibilities, we compared both the 1-vs-rest self-consistency and the prediction EV before and after removing the non-visual activity. Removing the non-visual ongoing activity increased the self-consistency value across the three mice (Figure Supplement 7C [↗](#);  $p < 0.001$ , paired permutation test). Interestingly, the inter-laminar EV fraction decreased in MP031 and MP032 mice, yet increased in MP033 (Figure Supplement 7F [↗](#)  $p < 0.001$ , paired permutation test). When examining individual pairwise relationships in a fraction of highly predictable neurons (lines in Figure Supplement 7F [↗](#)), we found that some of the highly predictable neurons remained predictable after removing the non-visual activity, whereas other highly predictable neurons dropped their EV fraction dramatically. Together with the small yet reliable shared behavior contributions (Figure Supplement 10), these results indicate that a non-trivial portion of inter-areal predictability in mice reflects shared internal-state fluctuations, whereas a complementary portion persists after removing those dimensions, consistent with stimulus-driven interactions.

In monkeys, one of the neuronal properties that showed high correlation with inter-areal prediction EV across all conditions was also the maximum correlation value (first column in Figure 6D, E [↗](#), Figure Supplement 8A [↗](#), and Figure Supplement 9 [↗](#)). Other neuron properties like SNR, split-half correlation, and one-vs-rest correlation were also highly correlated with inter-cortical predictability EV (Figure 6D [↗](#), Figure Supplement 8A [↗](#), and Figure Supplement 9A [↗](#)). The split-half correlation was highly correlated with EV fraction, although the relationship was highly non-linear (middle column in Figure 6D [↗](#), Figure Supplement 8B [↗](#), and Figure Supplement 9B [↗](#)). Using the one-vs-rest squared correlation removed some of this non-linearity and further increased the correlation with the EV fraction in monkeys L and A (third column in Figure 6D [↗](#), Figure Supplement 8B [↗](#)). In addition, the relationship between one-vs-rest correlation squared and EV fraction did not show evidence of bimodality ( $p = 0.99$ , Hartigan's dip test focusing on sites with  $EV > 0.4$ ).

We conjectured that neurons that have overlapping receptive fields (RFs) should share more information, and therefore their responses would better predict each other than neurons with non-overlapping RFs. In addition, even when all neurons are exposed to the same stimulus (full field symmetrical checkerboard image, gray screen, darkness, etc), neurons with overlapping RFs may be more synaptically connected, resulting in better inter-cortical predictions. To test this hypothesis, we compared inter-cortical predictions in different ensembles of neurons with RFs that differed in their degree of overlap. This hypothesis was only tested in monkeys L and A because we did not have access to RF estimates in the mouse data, and we did not have enough sites with RF overlap in monkey D. For each V4 site whose responses we predicted, we separated the predictors into two groups with matched size: one group where all the V1 predictor sites had <10% RF overlap (sample of one V4 site in monkey L, Figure 6F [↗](#), top), and one group where all the V1 predictor sites had >80% RF overlap (sample of one monkey L V4 site, Figure 6F [↗](#), bottom). A similar procedure was followed when predicting the activity of V1 neurons from V4 predictor neurons (Figure 6H [↗](#)). Inter-areal prediction was higher in the >80% RF overlap condition compared to the <10% RF overlap ensembles in both directions and across all stimulus conditions (Figure 6G, I [↗](#) for monkey L; Figure Supplement 8C, D [↗](#) for monkey A). To compare these numbers with those obtained with larger numbers of sites, we calculated the EV performance while using all predictors. In most cases, predictions using the >80% RF overlap group were lower than when using all predictors, showing that predictor neurons with low RF overlap still contributed to the EV (Figure 6G, I [↗](#), for monkey L; Figure Supplement 8C, D [↗](#) for monkey A).

## Inter-areal predictability is both stimulus and non-stimulus driven

The results in Figure 5 [↗](#) and Figure 6 [↗](#) pointed to components of the predictable responses that are stimulus-driven and other components that are not stimulus-driven. We considered two alternative hypotheses: (1) If shared information were strictly stimulus-driven, prediction across repeats of the same stimulus should remain accurate; (2) If shared information were entirely stimulus-independent, prediction across repeats should approach chance ( $EV \approx 0$ ). To test these

hypotheses, we compared the inter-areal prediction EV fractions using unshuffled versus shuffled trials. Shuffling was performed across repeat trials of the same images (mice: [Figure 7A](#), [monkeys: Figure 7D](#)). In mice, one stimulus presentation was either a drifting grating or a natural static image. In monkeys, one stimulus presentation was either the one checkerboard image, a large, thick, fast-moving bar, or a small, thin, slow-moving bar. In both species and in both directions, inter-areal prediction EV fraction decreased after shuffling stimulus repeats compared to before shuffling ([Figure 7B](#) for mouse; [Figure 7E](#) for monkey L; [Figure Supplement 11A](#) for monkey A; [Figure Supplement 11C](#) for monkey D;  $p < 0.001$  for both species and directions, paired permutation test).

Interestingly, the EV fraction during shuffled trial-repeats still remained significantly above chance ( $p < 0.001$ , paired permutation test of prediction vs. shuffled frames prediction). In mice, neurons showed two types of distribution in terms of their response predictability in shuffled and unshuffled trials. For a subset of neurons, the EV fraction was still high in the shuffled condition, albeit their EV was lower than in the unshuffled case ([Figure 7C](#); points below but near the diagonal line). For another subset of neurons, the EV fraction during shuffled trials was much lower or even near zero. The responses of the latter group had the highest predictability during gray screen activity.

In monkeys, neurons farther away from the diagonal line showed higher EV fraction during gray screen activity ([Figure 7F](#) for monkey L; [Figure Supplement 11F](#) for monkey A; [Figure Supplement 11G](#) for monkey D). In addition, we examined whether shuffling repeat presentations of gray screen images (simulating spontaneous activity) would result in any prediction at all. There was a more profound decrease in inter-cortical performance in all monkeys ([Figure Supplement 12A–C](#)) with no neurons that remained as predictable during shuffled trials compared to unshuffled trials ([Figure Supplement 12E–G](#)).

## Accounting for latency differences improves inter-areal activity predictions in monkeys visual area sub-populations

Given the latency differences in neuronal responses between V1 and V4 [Schmolesky et al., 1998](#), we asked whether accounting for this latency could result in better inter-cortical prediction. To test this hypothesis, we offset the neuronal activity using different lags for each area ([Figure 7G](#), [H](#)) and recalculated the ridge regression predictions. For each offset level, we calculated the percentage of neurons where the EV fraction peaked at that offset. For the checkerboard image, in monkeys L and A V1 → V4 predictions, the biggest percentage of neurons had a peak performance when there was no time offset between areas, with a substantial proportion of neurons with a peak performance for 10–30 ms offsets in the negative direction (i.e., V1 activity preceding V4 activity; [Figure 7I](#), left for monkey L, [Figure Supplement 11E](#), left for monkey A). This distribution of peak EV values was only present during early visual responses (first 275 ms of stimulus onset). In monkeys L and A V4 → V1 direction, there was a large proportion of neurons with peak EV when considering 10–20 ms offsets in the positive direction (i.e., V4 after V1, [Figure 7I](#), right for monkey L, [Figure Supplement 11E](#), right for monkey A). These differences were apparent in the early part of the visual response, before 250 ms. When offsetting the neuronal responses to gray screen presentations, across all times and areas, the highest percentage of neurons with peak EV was when there was no time offset ([Figure Supplement 12D](#)).

## Neural signals can also be predicted at the ensemble level using local field potential signals

We repeated the analyses in monkeys L and A using the local field potential (LFP) signals. We evaluated whether the predictability of LFP signals across areas depended on the signal frequency by considering band-limited LFP amplitudes (Low: 2–12 Hz; Beta: 12–30 Hz; Gamma: 30–45 Hz; High-gamma: 55–95 Hz; Hilbert envelopes, z-scored). In both monkeys, the Gamma band showed a feed-forward signature in the early evoked period: the V1 → V4 predictability peaked at negative offsets (~10–30 ms; V1 leads), and the V4 → V1 predictability peaked at positive offsets of similar

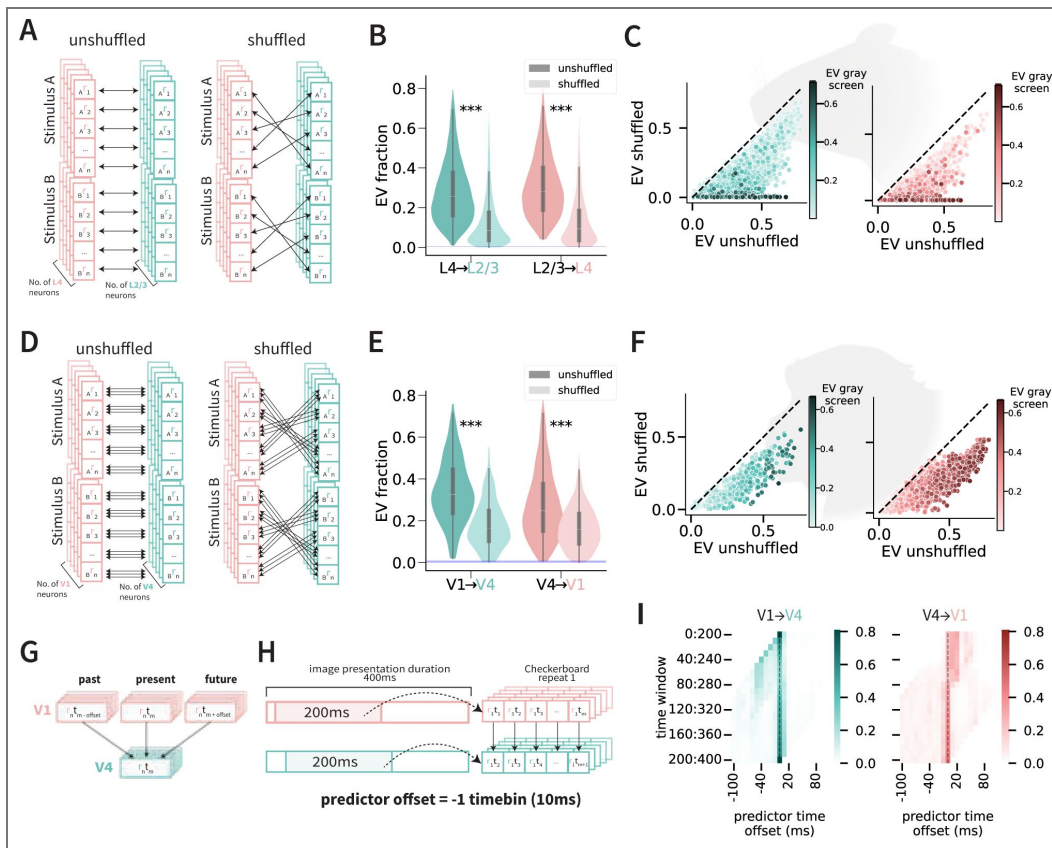


**Figure 7. Predicting neuronal activity across time reveals shared stimulus- and non-stimulus driven information in both mouse and monkey visual cortex, along with latency and non-latency specific correlations in monkey V1/V4.**

**A.** Shuffled-trial-repeat experiment set-up for comparing unshuffled vs. shuffled prediction in mouse V1 L2/3 and L4. Neuronal activity in response to stimulus repeats was shuffled within their respective image. **B.** EV fraction for unshuffled (dark) and shuffled (light) trials in the L4 → L2/3 (green) and L2/3 → L4 (coral) directions. **C.** Relationship between shuffled (y-axis) and unshuffled (x-axis) trial repeat EVs in the mouse L4 → L2/3 (left, green) and L2/3 → L4 (right, coral) directions. Hue represents EV fraction during gray screen activity. **D.** Shuffled-trial-repeat experiment set-up comparing unshuffled vs. shuffled prediction in monkey data. Neuronal activity (including all timepoints) in response to stimulus repeats was shuffled within their respective image. Since the checkerboard presentation was only one stimulus, the experiment visualization only applies to the “Stimulus A” portion. **E.** Same as **B** for monkey L V1 → V4 (green) and V4 → V1 (coral). **F.** Same as **C** for monkey V1 → V4 (green) and V4 → V1 (coral). **G.** Illustration of time offsets applied to monkey neuronal activity for inter-areal predictions. Instead of neuronal activity prediction between areas being done on simultaneous activity (middle coral and bottom green box), the V4 neuronal activity (green) at time  $t_m$  was predicted using V1 neuronal activity (coral) at time  $t_{m \pm offset}$ .  $t_{m \pm offset}$  were *offset* represents 1–8 timebins (25 ms per timebin) before (if negative; left coral box) or after (if positive; right coral box) time  $t_m$ . Time offset experiment was done in both prediction directions (V1 → V4 and V4 → V1). **H.** Experimental set-up example for predicting neuronal activity in V4 using V1 neuronal activity from 10 ms prior to V4 activity. Neural activity is in response to a repeated checkerboard image. A 200 ms section of the cortical area was used to represent the image presentation response, and was offset -1 timebin (10 ms) to predict a 200 ms target cortical area. During the prediction experiments, the 200 ms window was slid across the entire duration of the stimulus. **I.** Time offset prediction results across both V1 → V4 (left, green) and V4 → V1 (right, coral) prediction directions. Each square corresponds to the fraction of neuronal sites whose neural activity were best predicted during that offset period and time window.

magnitude [Figure Supplement 13A,D](#) for monkey L; [Figure Supplement 13B,E](#) for monkey A), consistent with previous findings ([Semedo et al., 2022](#); [van Kerkoerle et al., 2014](#); [Bastos et al., 2015](#)). The Low and Beta frequency bands exhibited a broader structure with less consistent peaks in predictability offset timing.

## Discussion

Neuronal activity in one brain region or layer within the visual cortex can be used to predict neuronal activity in another nearby and anatomically connected region or layer in single trials ([Figure 2](#)). In monkeys, predictability was asymmetric: V1 activity better accounted for V4 activity than vice versa ([Figure 3](#), [Figure 7](#)). This inter-areal prediction persisted across different stimuli ([Figure 4](#)) but also in the absence of a visual stimulus, during gray-screen and lights-off periods ([Figure 5](#)). The degree of predictability increased with signal-to-noise ratio, response variance, and the degree of overlap between receptive fields ([Figure 6](#)).

In line with other studies in mice ([Stringer et al., 2019b](#); [Niell and Stryker, 2008](#); [Andermann et al., 2011](#)), we observed an approximately bimodal distribution of neuronal responses, with a large subset of neurons that do not show reliable responses to visual stimuli both in L4 and L2/3 ([Figure 6B](#), third column; [Figure Supplement 7A](#)). However, even for the subset of neurons considered to be “non-visual”, at least within the set of stimuli and conditions examined here, their activity remains predictable. This bimodal distribution disappears when projecting out potential non-sensory ongoing activity ([Figure 6C](#); [Figure Supplement 7D](#)) ([Stringer et al., 2019b, 2021](#)). At the population level, neuronal encoding subspaces in mouse visual cortex have been shown to have little overlap between visual sensory and non-sensory (behavioral) information, with only one shared dimension ([Stringer et al., 2019b](#)). The visually unreliable, yet highly predictable, sub-set of neurons described here could be the neuronal group driving this orthogonality. As expected, the activity of “visual” neurons can be better predicted during visual presentation and not during gray screen presentation. In stark contrast, the activity of non-visual neurons can be predicted even better during gray screen presentation than during visual stimulation. There was no such bimodal distribution in the data from monkeys. One possibility is that there may be no (or very few) non-visual neurons in monkey V1 or V4. Indeed, the overwhelming majority of recording sites in V1 and V4 responded strongly to visual stimulation. Yet, the comparisons between the results in mice and monkeys reported here need to be interpreted with caution because the two datasets differ in terms of recording techniques (electrophysiology versus two-photon imaging), consequently also in their temporal resolution (one millisecond versus hundreds of milliseconds), and the type of interaction studied (across areas versus across layers), in addition to any differences between species.

In monkeys, sites where the receptive fields (RF) of V1 and V4 overlap can better predict each other compared to other sites showing little RF overlap. This observation could reflect RF-dependent intrinsic connectivity between areas, but also RF-dependent shared inputs from other areas, such as the thalamus. In the latter case, those putative shared inputs cannot be strictly dependent on visual inputs, given that the effect of RF overlap persists even during gray screen conditions.

Many computational models that aim to explain neuronal activity in the visual cortex are based on feedforward signal propagation, with increased receptive field sizes, selectivity, and feature invariance along the visual hierarchy ([Serre et al., 2007b](#); [Kreiman, 2021](#); [Connor et al., 2007](#)). Consistent with this idea, we described an asymmetry in the degree of predictability, with V1 neurons explaining V4 responses better than the other way around. This observation persisted after control-ling for neuronal count and split-half correlation values and was also apparent during the lights-off condition. In contrast, there was no asymmetry when comparing inter-laminar prediction directions in mice. The lack of asymmetry in inter-laminar prediction directions in mice could be due to the slow dynamics in calcium imaging, the lack of a clear inter-areal hierarchy, or differences between species.

The asymmetry in directionality was also observed when implementing temporal delays to inter-areal prediction, consistent with processing delays across areas (Semedo et al., 2022 [↗](#); Gokcen et al., 2022 [↗](#); Schmolesky et al., 1998 [↗](#)). A substantial proportion of neurons increased their inter-areal predictability when offsetting the times between areas, specifically in the direction that aligns their neuronal activities. In contrast to the temporal delays associated with processing visual stimulation, during gray screen presentation, the activity of most neurons was best predicted in the absence of any time offsets, suggesting that the internally generated neuronal activity during spontaneous conditions may be largely driven in a non-feedforward manner. Further evidence supporting the distinction between visually-driven and non-visually-driven interactions comes from the observation that trial repeat shuffling reduced, but did not eliminate, predictability in both mice and monkeys. In mice, when comparing shuffled versus unshuffled activity, we encountered again a bimodal distribution, where a group of neurons was closer to the diagonal line (their responses were predicted as well during the shuffled compared to the non-shuffled condition), and another group of neurons that were closer to the x-axis (their responses could not be predicted during the shuffled condition). The responses of the latter group were best predicted during gray screen activity, suggesting that they mostly shared non-visual information. The predictive power in mouse V1 from layer 4 to layer 2/3 during spontaneous conditions has been recently shown in Papadopouli et al. (2024) [↗](#), consistent with our findings. The overall area population decrease in predictability after shuffling may be due to the influence of non-visual activity, such as movement (Stringer et al., 2019 [↗](#) b), especially since these non-visual stimulus effects have been shown to occur on a timescale of approximately one second, consistent with the results in our study. In macaques, context-dependent effects are likely not due to movement, since the monkeys maintained fixation during the stimulus task, and visually-evoked activity was not driven by movement (Talluri et al., 2023 [↗](#)).

The neural recordings in mice and monkeys are different in terms of: (i) recording modalities (calcium versus electrophysiology), (ii) temporal resolution (hundreds of milliseconds versus milliseconds), (iii) neuronal types, (iv) SNR, (v) cortical targets (layers versus areas), (vi) sample sizes, (vii) stimuli, and (viii) task conditions (Stringer, 2018 [↗](#); Chen et al., 2022 [↗](#)). The goal of this study was not to make any direct quantitative comparison across species, but rather to investigate the properties of inter-areal interactions within each species.

Several limitations in this study are worth considering in future work. First, neither calcium imaging nor MUAe recordings capture the timing of single spikes in individual neurons. One of many ways in which the timing of individual spikes could be important is that synchronous or close-to-synchronous inputs can have a larger impact on post-synaptic responses (Salinas and Sejnowski, 2001 [↗](#)). Second, this study focused on linear predictability, but other non-linear models could better capture neuronal activity. Third, and critically, the experimental data evaluated here provide only a fraction of the inputs to a given neuron. For example, the predictor signals studied here are likely to exclude most (in monkeys) if not all (in mice) inhibitory inputs (Jiang et al., 2015 [↗](#); Shen et al., 2020 [↗](#); Ibrahim et al., 2020 [↗](#); Schuman et al., 2021 [↗](#)). Any cortical neuron receives extensive local inputs and non-local inputs from many other areas. Fourth, we only had limited access to non-visual sources that could contribute to predicting neuronal responses; other sources of input could include finer behavioral measurements, attention, familiarity, and arousal state. Finally, biophysically realistic models of the transformation between inputs and outputs of a given neuron should include their dendritic locations and specific synaptic potentials (Park et al., 2019 [↗](#); Petousakis et al., 2023 [↗](#)). Therefore, the quantitative results on the prediction of neuronal responses reported here constitute a lower bound.

We evaluated inter-areal interactions in different types of neuronal recordings, timescales, and species. These interactions were assessed in single trials, separating visually-driven and non-visual contributions, and accounting for the directionality and dynamics of neuronal responses. These efforts constitute an initial step towards, and a lower bound for, systematically building computational models that can account for the transformations from sensory inputs to their encoding across multiple processing steps in the cortex. Whereas many efforts with artificial

neural networks merely map inputs to outputs (Kreiman, 2021 [↗](#)), a detailed and systematic understanding of individual processing steps can lead to better and biologically more relevant computational models of sensory processing.

## Methods

### Datasets

We used the mouse dataset from (Stringer et al., 2019 [↗](#) a) containing calcium-imaging activity measurements from 43,630 neurons in layer 4 (L4) and 12,060 neurons in layers 2/3 (L2/3) in V1 of 4 mice during 32 different randomly interleaved presentations of either drifting gratings or gray-scale natural images (each one repeated more than 90 times), along with spontaneous activity during 30 minutes of exposure to a gray/black screen (Figure 1A [↗](#), data acquisition details in Stringer et al. (2019a,b) [↗](#)). Calcium imaging activity was recorded during stimulus presentations at a scan rate of 2.5 Hz or 3 Hz (each frame was acquired every 400 ms or 333 ms). The computed stimulus responses per stimulus presentation were averaged based on two frames immediately post stimulus onset. Cortical layers were determined using the 10-12 planar z-positions retrieved during the multi-plane calcium activity acquisition. For stimulus-response and spontaneous recordings, neuronal activity of each neuron was z-scored using its 30-minute gray screen spontaneous activity (mean gray-screen activity subtracted and divided by gray-screen activity standard deviation).

We used the dataset from Chen et al. (2022) [↗](#) for monkeys A and L and conducted new neural recordings from one additional monkey (monkey D). The Chen et al. dataset consists of envelope multiunit activity (MUAe) and LFP from 1,024 recording sites in one monkey (monkey L) in response to either multiple-day recordings of more than 60 repetitions of a full-size checkerboard image, moving small-thin or large-thick bars in 4 directions, gray screen presentations, or more than 30 minutes of baseline activity where the monkey was in a room with the lights off (Figure 1B [↗](#)). We also used data from a second monkey (monkey A) from the same published dataset. However, due to the degraded state of the electrodes at the time of the recording, we were only able to obtain enough data from V4 sites for responses to the full-size checkerboard image, moving bars, and gray screen presentations. Neuronal activity was summed over 25 ms non-overlapping bins. Activity duration was 300 ms, 400 ms, and 1 s for gray screen, checkerboard, and moving bar presentations, respectively. For the recordings during visual stimulation, the neuronal activity was normalized by subtracting the mean activity during the gray screen presentations separately for each site.

We collected new data from an additional monkey in response to the full-size checkerboard image presentations, gray screen presentations, and lights-off activity (~15 minutes). Monkey D (12 years old, 14.4 kg) was chronically implanted with floating multielectrode arrays (Microprobes for Life Sciences, MD) targeting areas including V1 and V4. Arrays consisted of 16 channels per area, yielding a total of 32 electrodes (V1-16, V4-16). All procedures received ethical approval by Harvard Medical School Institutional Animal Care and Use Committees and conformed to NIH guidelines provided in the Guide for the Care and Use of Laboratory Animals. All relevant ethical regulations for animal and nonhuman primate testing and research were followed.

The same conditions of stimulus presentation (image/square size, presentation time, etc) were presented as in Chen et al. (2022) [↗](#). Stimulus presentation and data acquisition (including electrophysiology and eye tracking) were coordinated using MonkeyLogic2 software (Hwang et al., 2019) and OmniPlex Neural Recording Data Acquisition Systems (Plexon Inc.), integrated via custom MAT-LAB scripts. Online spike sorting was performed with the PlexControl client using waveform-based classification. Visual stimuli were displayed on ViewPixx EEG monitors (ViewPixx Technologies; 1920×1080, 120 Hz), and eye position was monitored via ISCAN (ISCAN Inc.). Raw analog signals were used to calculate MUAe using same processing logic as Chen et al. (2022) [↗](#).

## Visual Reliability

A neuron or site was defined to be visually reliable if its signal-to-noise ratio (SNR) was 2 or higher and its split-half correlation value was 0.8 or higher. Due to the high number of repetitions of visual stimuli, the split-half correlation was skewed toward high values, which is why we used a higher split-half correlation threshold than commonly used in other studies. In mice, the SNR for each neuron was calculated as:

$$SNR_{\text{mouse}} = \frac{\langle r_{\text{stim}} \rangle - \langle r_{\text{spont}} \rangle}{\text{std}(r_{\text{spont}})} \quad (1)$$

where  $\langle \rangle$  denotes mean,  $\text{std}$  denotes the standard deviation,  $r_{\text{stim}}$  is the average activity in response to stimuli, and  $r_{\text{spont}}$  indicates the average activity over the 30-minute gray screen presentation.

In monkeys, we followed the definition in [Chen et al. \(2022\)](#) and calculated the SNR for each site as:

$$SNR_{\text{monkey}} = \frac{\max(\langle r_{\text{stim}} \rangle) - \langle r_{\text{spont}} \rangle}{\text{std}(r_{\text{spont}})} \quad (2)$$

using the peak activity during the checkerboard presentation for the signal, and the average gray screen neuronal activity as background (denoted as  $r_{\text{spont}}$ ).

In mice, the split-half consistency was calculated by correlating the average activity for the 32 stimuli in half of the trials, randomly chosen, with the average activity in the other half of the trials, followed by Spearman-Brown correction (used to correct for the division of trials by half). In monkeys, during checkerboard presentations, the split-half consistency was calculated by correlating the average activity of the 16 timepoints (0–400 ms; 25 ms bins) of checkerboard presentation of 25 random trial repetitions with the average activity of another non-overlapping 25 random repetitions, followed by Spearman-Brown correction. During moving bar presentations, the 40 time-points (0–1s; 25 ms bins) during 25 random trial repetitions were first concatenated across the 4 directions (total of 160 timepoints), and then correlated to the concatenated averaged activity of another nonoverlapping 25 random trial repetitions, followed by Spearman-Brown correction. For all split-half consistency calculations, we randomly sampled trials 20 times.

## Inter-areal predictions

Let  ${}_A r_{i,t}$  be the activity of neuron or site  $i$  in area  $A$  at timepoint  $t$ , where  $A$  can be L4 or L2/3 in the mouse data and V1 or V4 in the monkey data. Neuronal activity from one area (e.g., mouse V1 L4 or monkey V1) was used to predict activity in the other area (e.g., mouse V1 L2/3 or monkey V4) using ridge regression ([Figure 1E](#)). The activity of each neuron  $i$  in area  $A_2$  was predicted from  $n_{A_1}$  neurons in area  $A_1$  as follows:

$${}_{A_2} \hat{r}_{i,t} = \sum_{j=1}^{n_{A_1}} w_{i,jA_1} r_{j,t} + b_i \quad (3)$$

During fitting, we minimized the residual sum of squares (RSS), defined as:

$$RSS_i(\mathbf{w}, b_i) = \sum_{t=1}^{n_T} ({}_{A_2} \hat{r}_{i,t} - {}_{A_2} r_{i,t})^2 + \alpha \sum_{j=1}^{n_{A_1}} w_j^2 \quad (4)$$

where  $\mathbf{w}$  is the weight vector for predicting the activity of neuron  $i$ ,  $n_T$  is the number of images/time points and  $\alpha$  controls the regularization strength ( $\alpha$  was tuned for each dataset

with an independent sample and ranged from  $10^3$  to  $10^5$ ). Predictability for each neuron was evaluated using 10-fold cross-validation across trials and quantified as squared Pearson's  $r$  between held-out  $_{A2}r_{i,t}$  and  $_{A2}\hat{r}_{i,t}$ , referred to as explained variance fraction (EV fraction) throughout.

To remove temporal auto-correlation that would inflate the apparent prediction despite cross-validation, we removed training timepoints near the test timepoints closer than the decay window of the activity auto-correlation (mouse: 5 s; monkey: 1.5 s). The auto-correlation decay window was determined using time-series forecasting Ridge Regression (using  $r_t$  to predict  $r_{t+d}$ , where  $d$  represents a delay). The delay was increased until the EV fraction approached chance.

To model a Poisson distribution of MUAe responses, we also fit a Poisson generalized linear model (GLM) using the same predictors as above.

We implemented this model with scikit-learn's PoissonRegressor (log link; intercept  $b_i$  unpenalized) and tuned  $\alpha$  per dataset using an independent sample. Model evaluation followed the same 10-fold cross-validation and temporal exclusion procedure as ridge regression (1.5 s exclusion window for monkey). Predictability was quantified as the squared Pearson correlation between observed and predicted MUAe on held-out folds (EV fraction), allowing direct comparison between ridge regression and Poisson GLM (Figure Supplement 1M [↗](#)).

## Prediction directionality

We compared predictability across layers in different directions (in mice: L4 → L2/3 vs. L2/3 → L4) and also predictability across areas in different directions (in mon-keys: V1 → V4 vs. V4 → V1) (Figure 3 [↗](#)). To ensure that results were not dependent on the number of neurons/sites, we randomly subsampled the number of neurons/sites of the area containing the larger number of neurons/sites (L2/3 for mouse; V1 for monkeys) to match the number of predictors in both directions (10 iterations per recording type, neuron count details in Table 1 [↗](#) and Table 2 [↗](#)). Results in Figure 3 [↗](#) represent the median across the 10 subsamples). To account for potential changes in intrinsic predictability, we ensured that the neurons from both areas were matched in terms of the distribution of split-half correlation values so that the difference between individual area neurons/sites was less than 0.002. To assess the intrinsic predictability of neurons/sites in each region, the areas were used to predict themselves, where one neuron/site in the area was predicted by the remaining neurons in the same area. This “intra-areal” prediction was used to normalize EV fraction to compare directionality of prediction.

## Stimulus types and spontaneous activity comparison

We compared predictability for different stimulus conditions (Figure 4 [↗](#), Figure 5 [↗](#)). To compare inter-areal prediction across stimulus types and between the presence or absence of stimuli, the number of predictors (neurons or sites) and timepoints was sub-sampled to be the same across all datasets. In monkeys, the time spent recording the lights-off condition was much greater than during stimulus or gray screen presentations. To account for the difference in time duration and therefore training size, we subsampled time periods to be the same across all stimulus, gray-screen, and lights-off, lights-off eyes open, and lights-off eyes closed conditions.

## Neuron properties

We compared different neuronal properties with predictability measurements (Figure 6 [↗](#)). The SNR and split-half correlation has been defined above. The absolute max pairwise correlation value of each neuron/site  $i$  in one area with all neurons in the other area was calculated as

$$_{A2} \text{maxcorr}_i = \max_j (|\text{corr}(_{A2}r_i, _{A1}r_j)|) \quad (5)$$

where  $_{A2}r_i$  represents the activity of neuron/site  $i$  in area A2, which are correlated with the activity of every neuron  $j$  in area A1 (denoted as  $_{A1}r_j$ ).

One-vs-rest self-consistency (1-vs-rest  $r^2$ ). For each neuron/site  $i$  with  $T$  repeat trials, let  $r^{(t)} \in \mathbb{R}^M$  be its activity vector from repetition  $t$  across all stimuli/timepoints (length  $M$ , defined below). The leave-one-out mean response over repetitions *excluding*  $t$  is

$$\bar{\mathbf{r}}_i^{(rest)} = \frac{1}{T-1} \sum_{\substack{t'=1 \\ t' \neq t}}^T \mathbf{r}_i^{(t')}$$

Throughout, the superscript (*rest*) means “all repetitions excluding repeat  $t$ ”.

The one-vs-rest correlation for the held-out repetition  $t$  is

$$SC_i^{(t)} = \text{corr} \left( \mathbf{r}_i^{(t)}, \bar{\mathbf{r}}_i^{(rest)} \right), \quad (7)$$

We then average these correlations across all held-out repetitions:

$$\overline{SC}_i = \frac{1}{T} \sum_{t=1}^T SC_i^{(t)}. \quad (8)$$

In mice,  $r^{(t)}$  stacks the responses to the  $S = 32$  stimuli for repetition  $t$  (each element is the mean of the two frames immediately post-onset). In monkeys, during checkerboard presentations,  $r^{(t)}$  stacks the  $T = 16$  timepoints (0–400 ms; 25 ms bins). In monkey moving-bar presentations,  $r^{(t)}$  concatenates the  $T = 160$  timepoints (4 directions  $\times$  40 bins; 0–1 s, 25 ms bins).

Variance metrics. All variances were computed on gray-baseline-subtracted signals. In mice (32 gratings,  $K$  repeats), for neuron  $i$ , let  $r^{(k,s)}$  denote the scalar response to stimulus  $s \in \{1, \dots, S\}$  on repeat  $k \in \{1, \dots, K\}$  (repeat-averaged within the analysis window). We defined:

$$\begin{aligned} \bar{r}_i^{(s)} &= \frac{1}{K} \sum_{k=1}^K r_i^{(k,s)} \\ v_i^{\text{trial}} &= \frac{1}{S} \sum_{s=1}^S \text{Var}_k \left( r_i^{(k,s)} \right) \end{aligned}$$

In monkeys, for the checkerboard stimuli, for site  $i$  let  $r^{(k,t)}$  denote the scalar response to timepoint  $t \in \{1, \dots, T\}$  on repeat  $k \in \{1, \dots, K\}$

$$\begin{aligned} \bar{r}_i^{(t)} &= \frac{1}{K} \sum_{k=1}^K r_i^{(k,t)} \\ v_i^{\text{across}} &= \frac{1}{T} \sum_{t=1}^T \text{Var}_k \left( r_i^{(k,t)} \right) \end{aligned}$$

In monkeys, for the moving bar stimuli, the same two metrics were computed per stimulus  $s$  and then averaged across the four stimuli. In addition, we defined an across-stimuli variance of the time-averaged, trial-mean response:

$$v_i^{\text{stim}} = \text{Var}_s \left( \bar{r}_i^{(s)} \right), \quad \text{where } \bar{r}_i^{(s)} = \frac{1}{K} \sum_{k=1}^K \left( \frac{1}{T} \sum_{t=1}^T x_i^{(k,s)}(t) \right), \quad (13)$$

These variance covariates (together with SNR, split-half self-consistency, and one-vs-rest  $r^2$ , where applicable) were included as regressors in the *within-dataset-type* linear models used to obtain residual explained variance,  $EV_{\text{resid}} = EV - \hat{E}V$ .

## EV residualization

For each direction (V1  $\rightarrow$  V4, V4  $\rightarrow$  V1) and stimulus, we fit an ordinary least squares (OLS) model:

$$\widehat{EV}_i = \beta_0 + \beta_1 \text{SNR}_i + \beta_2 (\text{split-half } r_i) + \beta_3 \text{Var}_{\text{time},i} + \beta_4 \text{Var}_{\text{trials},i} + \varepsilon_i \quad (14)$$

where  $EV_i^\wedge$  is the predicted explained variance of each neuron/site  $i$ . Predictors were z-scored within each direction or stimulus.  $\text{SNR}_i$  is its signal-to-noise ratio (defined in the *Visual Reliability* section), split-half  $r_i$  is its split-half consistency (also defined above),  $\text{Var}_{\text{time},i}$  and

$\text{Var}_{\text{trials},i}$  are the temporal and across-trial variance metrics (defined in the *Variance metrics* section),  $\beta_0, \dots, \beta_4$  are regression coefficients, and  $\epsilon_i$  is the residual error term. Predictors were z-scored within each direction or stimulus. Residual EV was defined as  $EV_{\text{resid},i} = EV_i - \hat{EV}_i$  and used for all post-adjustment comparisons (Figure Supplement 3E–H [↗](#); Figure Supplement 5K,O [↗](#)).

## Dip test of unimodality

We used Hartigan's dip test to evaluate whether the distribution of 1-vs-rest squared correlation values was unimodal or not (Figure Supplement 7A,D [↗](#)). The test was performed after restricting the analysis to highly predictable neurons/sites ( $EV > 0.4$ ). The dip statistic measures the maximum deviation between the empirical cumulative distribution function and the closest unimodal distribution (Hartigan and Hartigan, 1985 [↗](#)). Reported  $p$ -values correspond to the probability of obtaining a dip statistic at least as large under the null hypothesis of unimodality. Dip tests were computed separately for each cortical layer and mouse (Python package `dipTest`).

## Receptive field overlap comparisons

In monkeys L and A, receptive field (RF) ellipses were calculated using center and edge locations in the dataset (Figure 6E, F [↗](#)). To calculate the percentage of RF overlap between the neuronal sites to be predicted and the predictor, the intersection area between ellipses was retrieved using the Shapely Python package, and divided by the area of the predicted site. Sites that had predictors that overlap both more than 80% and less than 10% were selected to compare inter-areal predictions. To control for predictor size, 14 random predictor sites from all the sites in each overlap type were subsampled (10 random samples without replacement).

## Trial repeat shuffling and time offset predictions

For the shuffled-trial experiments, we shuffled the predictor activity across repeat trials showing the same stimulus (Figure 7 [↗](#)). Thus, the stimulus order remained the same. For the mouse time-offset analysis, the activity of predictor neurons was time-shifted in the positive or negative direction, with 1 bin corresponding to 1 stimulus presentation (800–900ms). For the monkey dataset, the predictor activity (400 or 1000 ms per presentation, 16–50 bins of 10 ms each) was offset across time bins. We used sub-windows of 200 ms to avoid window-length differences that would otherwise be introduced if we shifted the entire trial response.

Supplemental Material

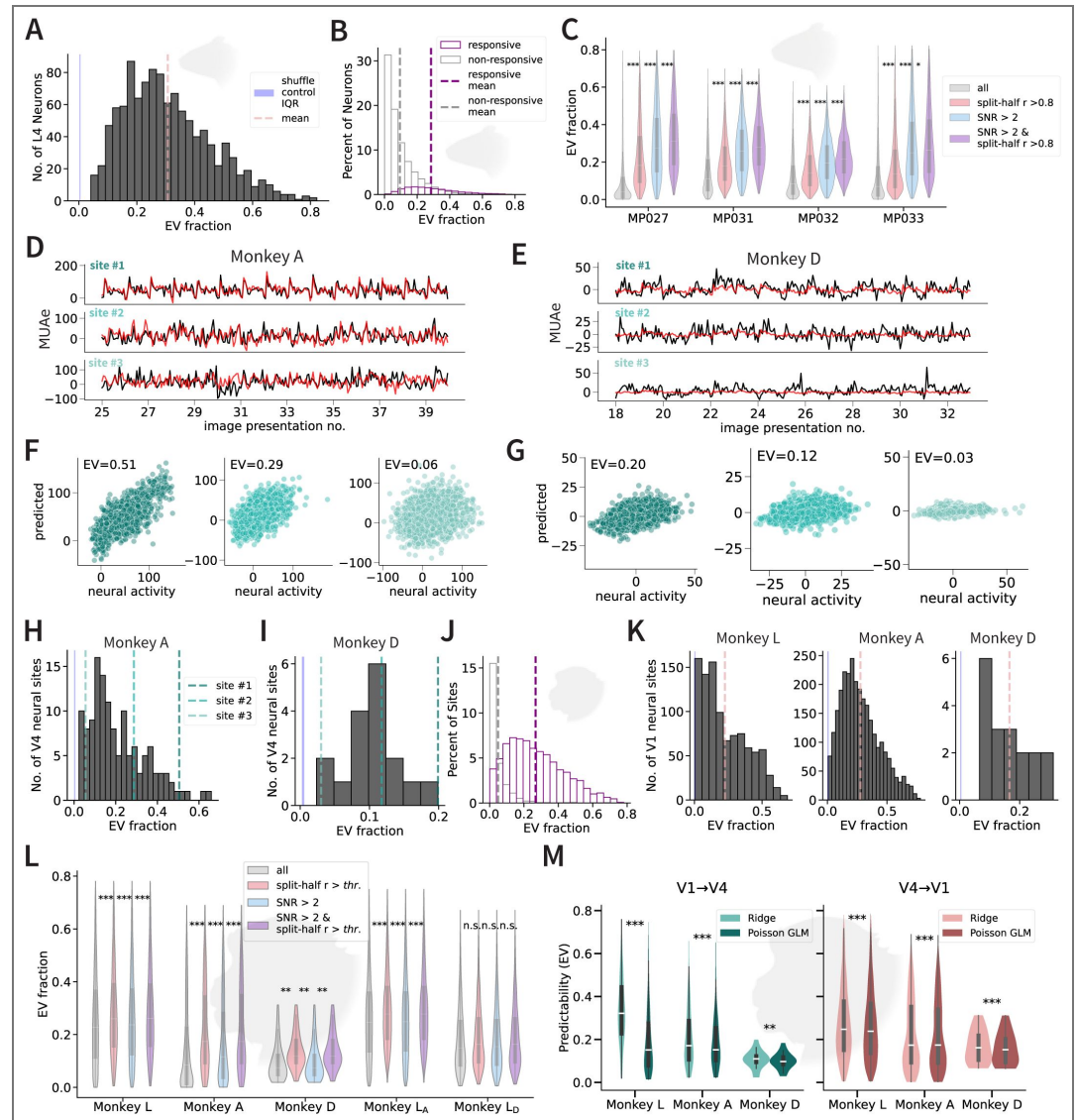
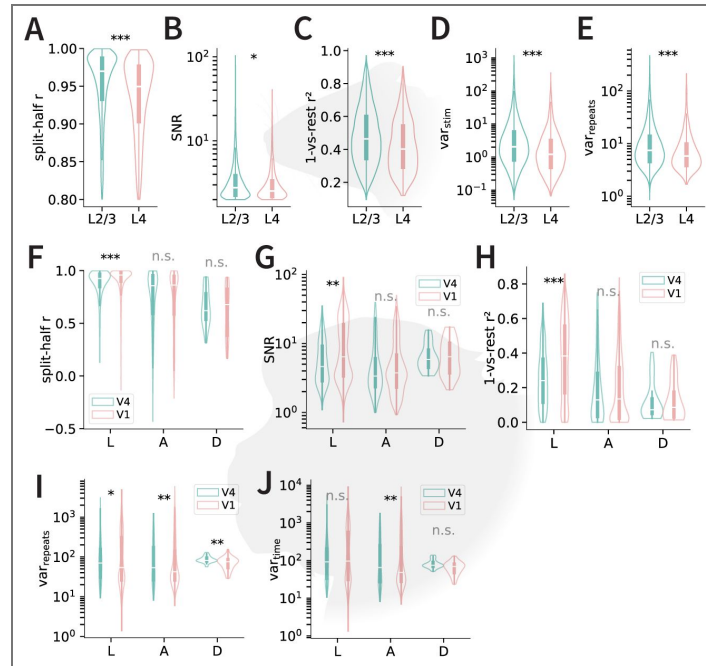


**Figure Supplement 1. EV fraction in mouse L4 neurons and monkey V1 neuronal sites and comparison between visual and non-visual neurons/sites.** **A.** Distribution of EV fraction in L2/3 – L4 regressions in cells deemed visually reliable in 4 mice and 7 recording days ( $n = 1113$  neurons). **B.** Distribution of EV fraction values for visually (purple) and non-visually (gray) reliable neurons in mouse L2/3 and L4. In mice, we used a conservative criterion to select neurons that were visually reliable, based on an average signal-to-noise ratio over 2 and a split-half correlation value of at least 0.8 (Methods). **C.** Differences in EV fraction using different filtering methods to determine visually reliable neurons in mouse L2/3 and L4 across the 4 mice. **D.** Example of monkey A MUAe activity (black) in response to a full-field checkerboard image in three V4 neuronal sites along with regression-model predictions (red) for a typical site (2, middle), site in the top 10% percentile of predictability (1, top), and bottom 10% percentile (3, bottom). **E.** Same as **D** for monkey D. **F.** Predicted neuronal activity versus actual neuronal activity in response to checkerboard and moving bar presentations for monkey A sites 1, 2, and 3 shown in **D**. Each point represents activity in one 2×5 ms timepoint during the 400 ms presentation. **G.** Same as **F** for monkey D neuronal sites shown in **E**. **H.** Distribution of EV fraction in V1 → V4 regressions of neural activity in response to visual stimuli in sites deemed visually reliable in monkey A (3 recording days, 30–44 V4 sites recorded per day;  $n = 132$  total site recordings). **I.** Same as **H** for monkey D (2 recording days, 7–10 V4 sites recorded per day;  $n = 17$  total site recordings). **J.** Distribution of EV fraction for visually (purple) and non-visually (gray) reliable neurons in monkey V1 and V4. Both SNR over 2 and a split-half correlation value of over 0.8 were used to define a

neuron to be visually reliable in monkeys L and A. In monkey D, a lower split-half correlation value of 0.6 was used to increase the site count. **K.** Distribution of EV fraction in V4 → V1 regressions of neural activity in response to visual stimuli in sites deemed visually reliable in monkeys L (5 recording days, 537–592 V1 sites recorded per day;  $n = 2789$  total site recordings), A (3 recording days, 251–381 V1 sites recorded per day;  $n = 989$  total site recordings), and D (2 recording days, 8–10 V1 sites recorded per day;  $n = 18$  total site recordings). **L.** Differences in EV fraction using different filtering methods to determine visually reliable neurons in macaque V4 and V1 across three monkeys (L, A, and D) V1 and V4 sites and two subsampled permutations of monkey L (to compare to site counts in monkey A and D). Split-half correlation value  $t\bar{r}$  represents either 0.8 (monkeys L, A, and  $L_A$ ) or 0.6 (monkey D and  $L_D$ ). **M.** Head-to-head comparison of ridge regression EV and Poisson GLM EV on monkey MUAe for V1 → V4 (left) and V4 → V1 (right). Models share identical train/test folds, 25 ms bins, and temporal gaps; the Poisson GLM enforces non-negativity via a log link on raw MUAe (no baseline subtraction).

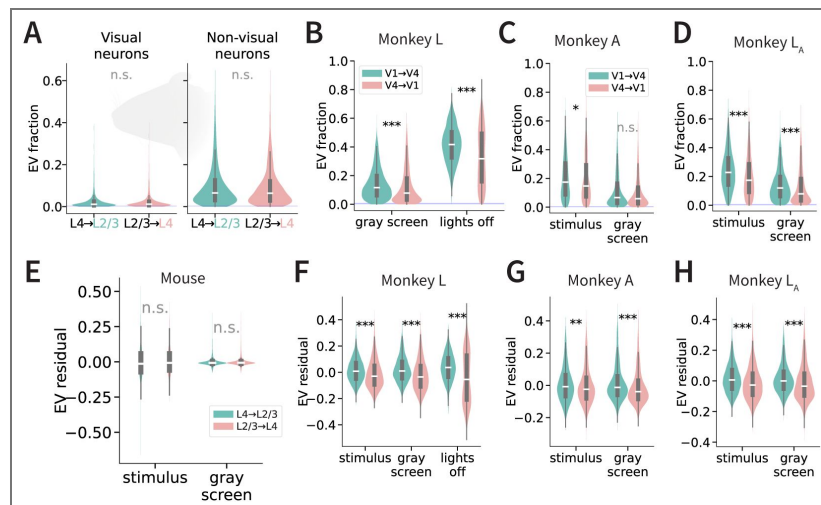
**Figure Supplement 2. Neuronal property differences between areas in mouse and monkeys.**

**A–E.** Differences in self-consistency, SNR, 1-vs-rest squared, variance across stimuli, and variance across repeats between entire visually reliable neuronal populations in mouse L2/3 and L4. **F–J** Differences in self-consistency, SNR, 1-vs-rest squared, variance across time (within repeat), and variance across repeats (within timepoint) between entire visually reliable neuronal populations in monkey V1 and V4.



**Figure Supplement 3. Differences in monkey inter-cortical predictability directions and lack of difference in mouse inter-laminar predictability directions are also seen in the absence of a stimulus.**

**A.** Differences in inter-laminar predictability directions in mouse neuronal activity during gray screen presentation in visual (left) and non-visual (right) neurons. **B.** Differences in inter-cortical predictability directions in monkey L during gray screen presentation and during lights off conditions. **C.** Differences in inter-cortical predictability directions in monkey A during stimulus and gray screen presentation. **D.** Same as **C** but for monkey L, after subsampling to match the number of sites in monkey A ( $L_A$ ). **E.** Differences in EV residuals after removing target-population covariates in mouse neural activity during stimulus and gray screen presentation (self-consistency, SNR, one-vs-rest  $r^2$ , and variance metrics; for details see Methods). **F** Same as **E** but for monkey L EV residuals during stimulus, gray screen, and lights off conditions. **G.** Same as **E** but for monkey A EV residuals during stimulus and gray screen conditions. **H.** Same as **G** but for monkey L, after subsampling to match the site counts of monkey A ( $L_A$ ).



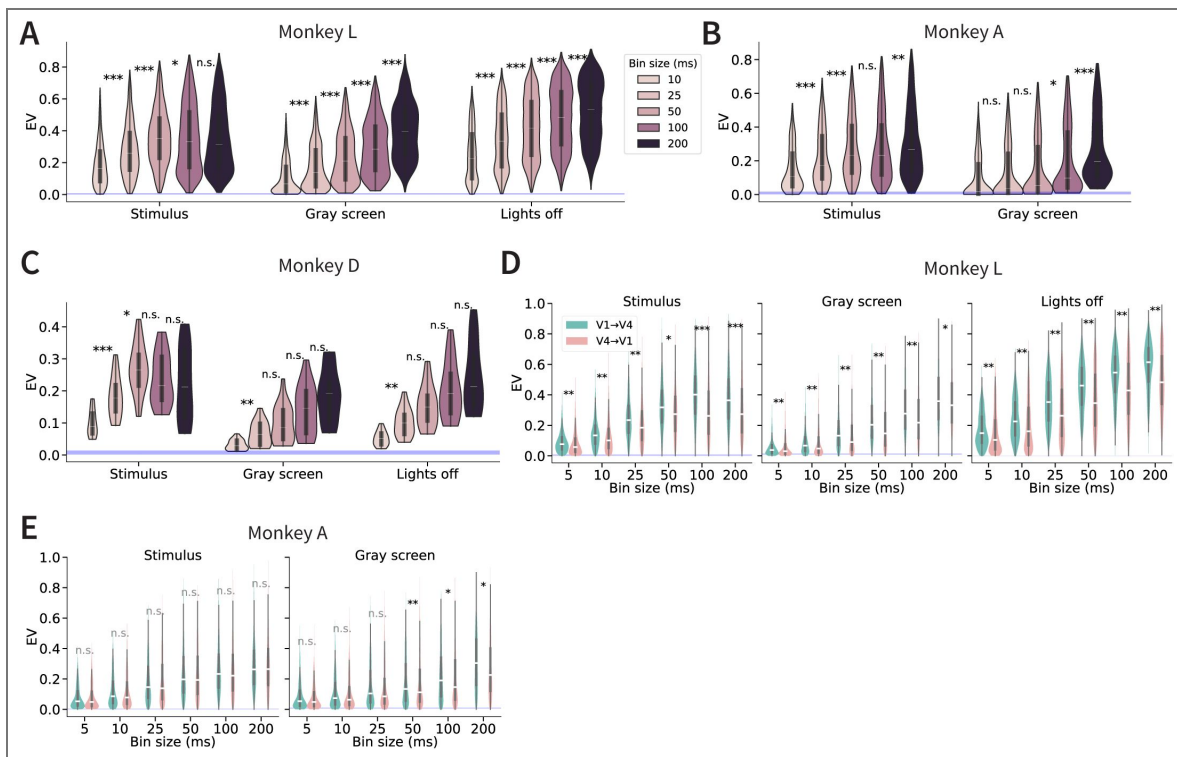


**Figure Supplement 4. Inter-areal predictability across bin sizes.**

A. Distribution of EV fraction for V1 → V4 predictions in monkey L across stimulus, gray screen, and lights off conditions. Each violin plot corresponds to a different bin size (10–200 ms; color legend). B. same as A but for monkey A stimulus and gray screen conditions. C. Same as A but for monkey D. D. Same conditions as in A, but with sites randomly sub-sampled as in Fig. 3 to match both the number of sites and the distribution of split-half reliability values across the two prediction directions (V1 → V4, teal; V4 → V1, coral). E. Same as D but for monkey A stimulus and gray screen conditions.

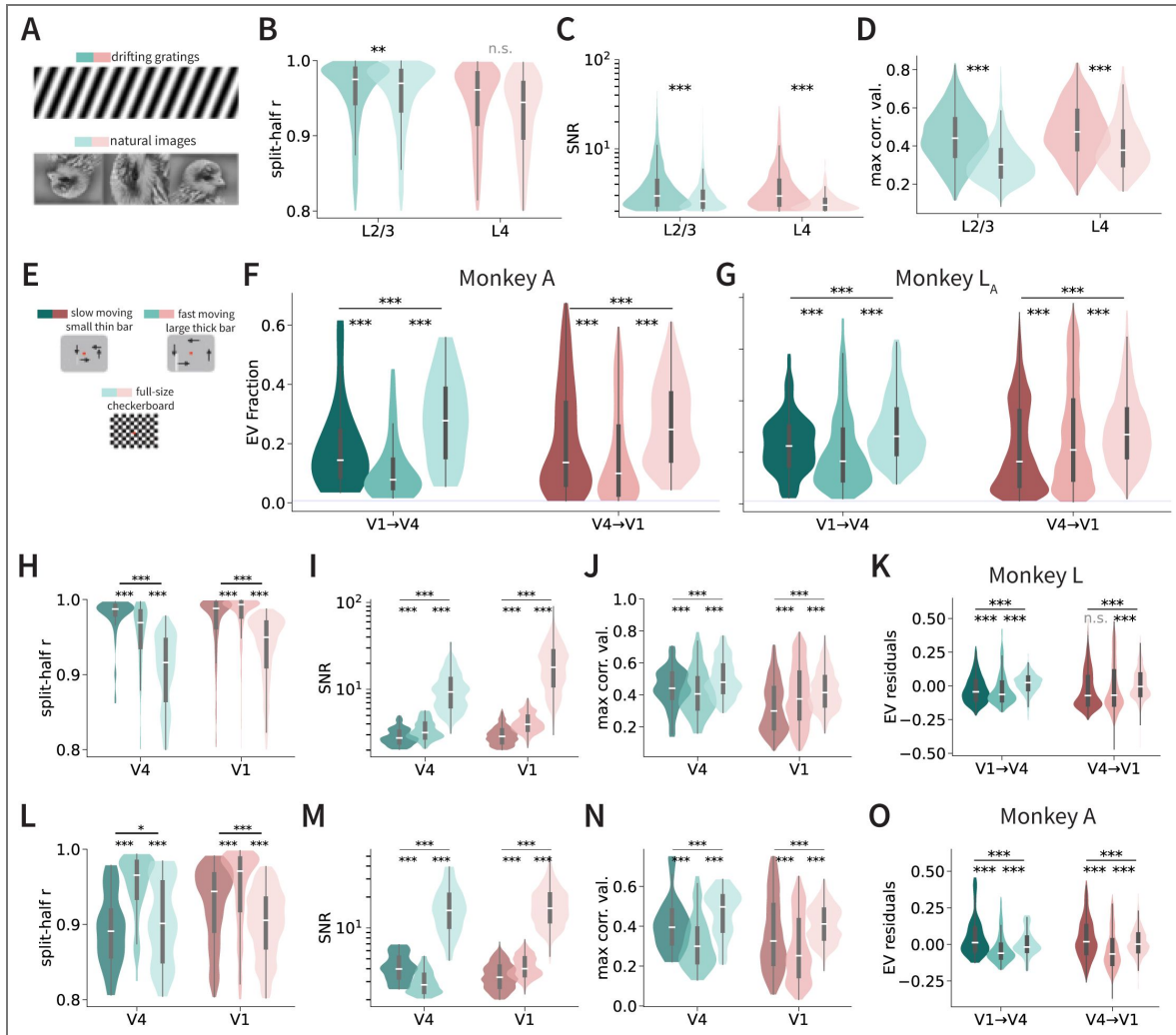


**Figure Supplement 5. Neuronal activity properties for different stimulus types.**

**A.** Sample stimuli for mouse drifting grating and static natural images. **B-D.** Split-half correlation (**B**), SNR (**C**), and maximum correlation values (**D**) for each mouse layer and stimulus type (see color scheme in **A**). **E.** Sample stimuli for monkeys: full-size checkerboard, slow and fast moving bars. **F.** Across-area predictability for each stimulus type (dark: slow bars, medium: fast bars, light: checkerboard) and direction for monkey A. **G.** Same as **F** but for subsampled monkey L ( $L_A$ ). **H-I.** Same as **B-D** for monkey L V1 and V4 (see color map for each stimulus condition in **E**). **K.** EV residuals for monkey L after regressing, within direction, on SNR, split-half reliability, variance across time (within stimulus), and variance across trials (within timepoint). **L-N.** Same as **B-D** but for monkey A V1 and V4. **O.** Same as **K** but for monkey A.

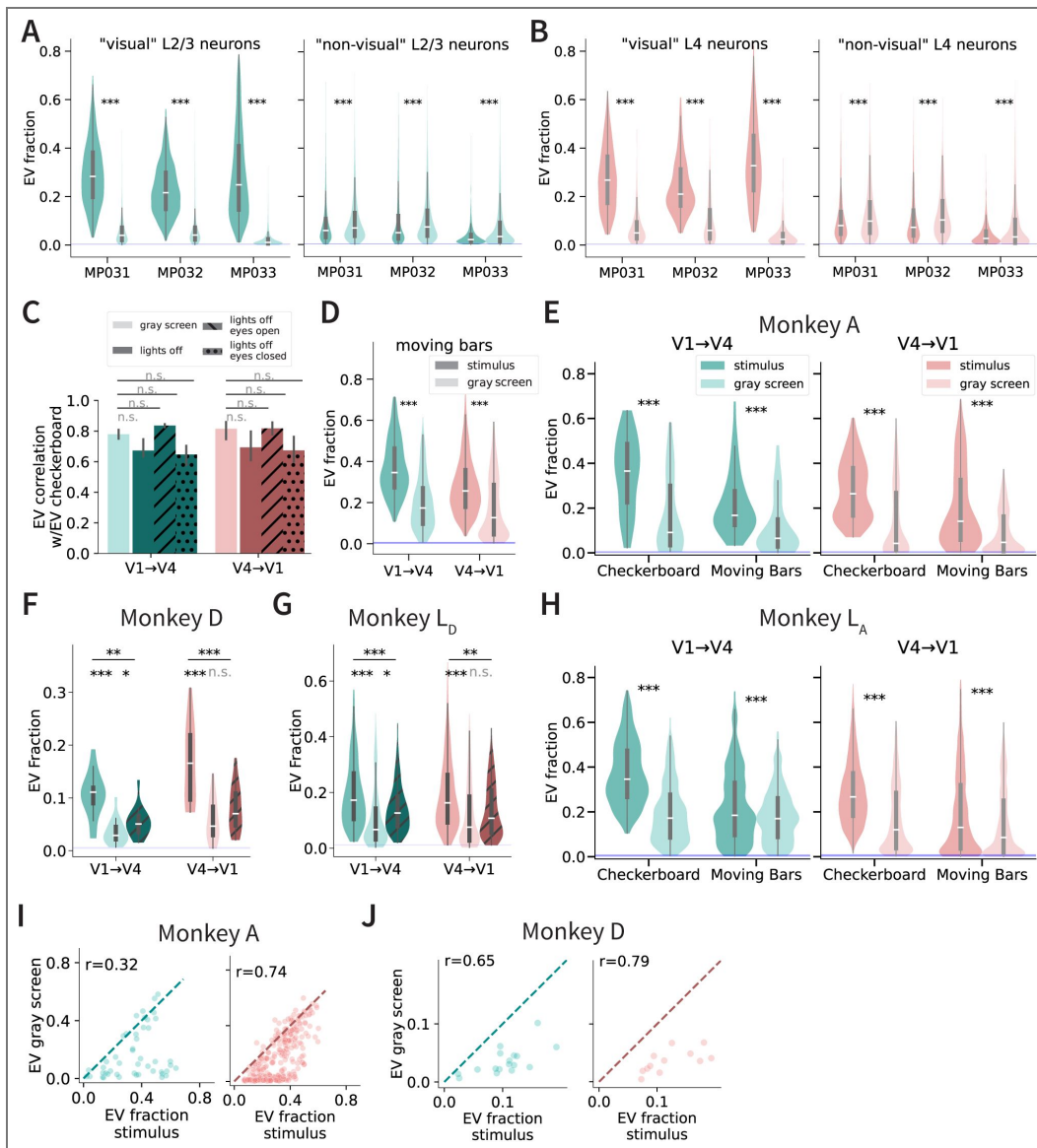


**Figure Supplement 6. Comparing stimulus presentation vs. gray screen activity predictions in mouse and monkey.**

**A.** Differences in inter-laminar predictability between stimulus presentation and gray screen presentation neuronal activity in L4 → L2/3 predictions across the three different mice (MP027 did not undergo gray screen presentation recordings). Left: visually reliable L2/3 neurons. Right: non-visually reliable L2/3 neurons. **B.** Same as **A**, but for mouse L2/3 → L4 predictions. **C.** Correlation coefficient values between checkerboard presentation and gray screen and lights off conditions in monkey inter-cortical predictability. **D.** Differences in inter-cortical predictability between moving bar presentation and gray screen activity in monkey L V1 → V4 and V4 → V1 predictions (paired permutation test). **E.** Differences in inter-cortical predictability between stimulus and gray screen presentation across both checkerboard and moving bar stimuli in monkey A. **F.** EV differences in inter-cortical predictability between stimulus, gray screen, and lights off conditions in monkey D. **G.** Same as **F** but for monkey L subsampling sites to match the number of sites in monkey D ( $L_D$ ). **H.** Same as **E** but for monkey A, after subsampling sites to match the number of sites in monkey A ( $L_A$ ). **I.** Correlation between EV in responses to gray screen (y-axis) versus stimulus presentation (x-axis) in monkey A visually reliable neurons (V1 → V4:left, green; V4 → V1:right, coral). The diagonal line represents the line of equality ( $y=x$ ).  $r$  is the Pearson's correlation coefficient. **J.** Same as **I** for monkey D.

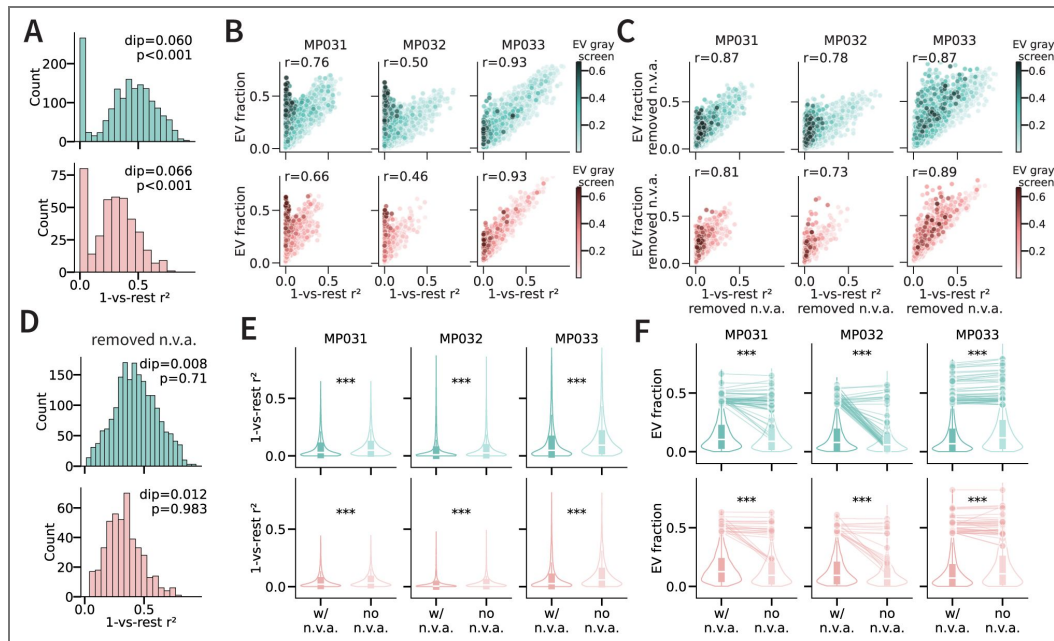


**Figure Supplement 7. Properties of visual and nonvisually active neurons in mice.**

**A.** Bimodal distribution of 1-vs-rest squared correlation values in highly predictable L2/3 (top) and L4 (bottom) neurons ( $EV > 0.4$ ). Hartigan’s dip test was applied to test bimodality (top right corner). **B.** Relationship between 1-vs-rest squared correlation and EV fraction in L2/3 (top, green) and L4 (bottom, coral) neurons in three mice (columns). **C.** Same as **B** after projecting out “non-visual ongoing” activity (Stringer et al., 2019), see text for details. **D.** Distribution of 1-vs-rest squared correlation values in highly predictable L2/3 (top) and L4 (bottom) neurons ( $EV > 0.4$ ) after projecting out “non-visual ongoing” activity. **E.** One-vs-rest squared correlation values when including (left) and not including (right) non-visual ongoing activity in each mouse (columns). \* denote paired permutation test. **F.** EV fraction when including (left) and not including (right) non-visual ongoing activity dimensions in L2/3 (top, green) and L4 (bottom, coral) in each mouse (columns). Sample subset of neurons with initial prediction values of over 0.4 visualized with lineplots. \* denote paired permutation test.

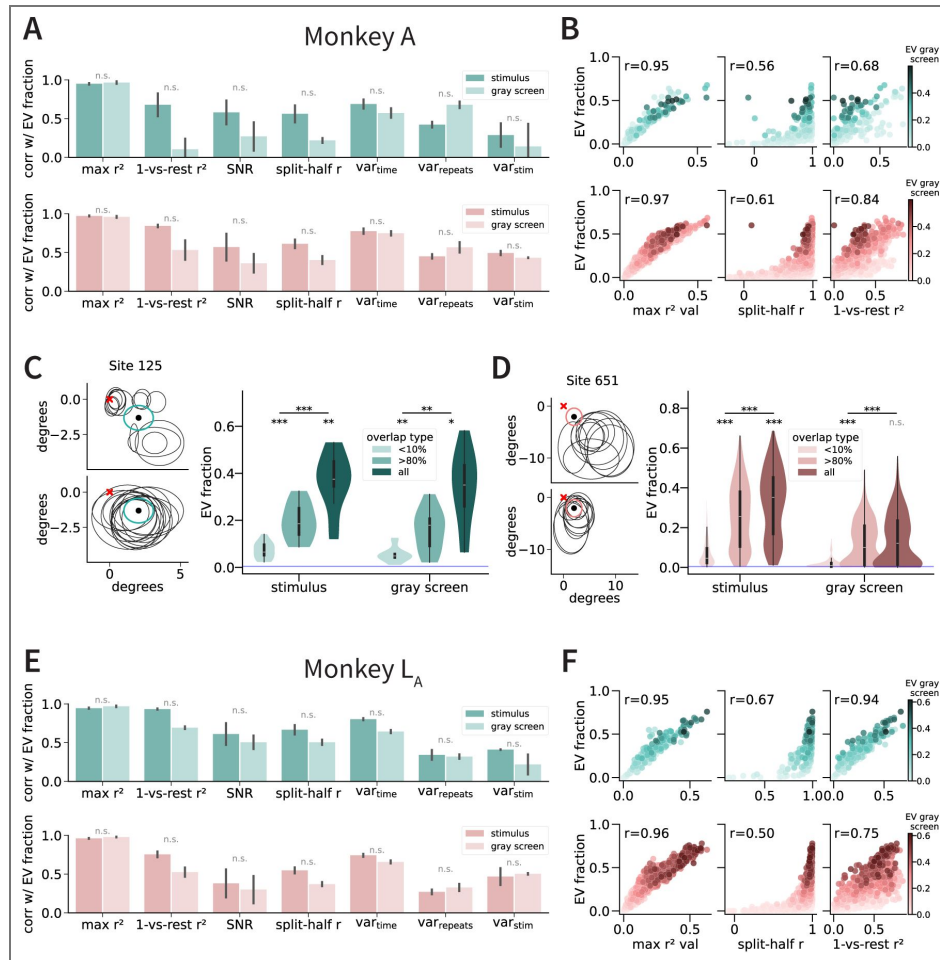


**Figure Supplement 8. Influence of SNR, variance, and receptive field overlap is consistent across monkeys L and A.**

**A.** Correlation between different properties with the predictability of V4 (green) and V1 (coral) neuronal responses during the presence (dark color) or absence (light color) of visual stimulus in monkey A. **B.** Relationship between the EV fraction and three neuronal properties in sites for monkey A V4 (green) and V1 (coral) responses to visual stimuli. Hue represents the degree of predictability for the same sites during gray screen presentations (see color scale on right). **C.** Left, top: Receptive fields of one sample V4 neuronal site in monkey A (green circle, array 2 electrode 187) and 14 randomly selected V1 neuronal sites as predictors (black circles), constrained on sites that share less than 10% receptive field overlap with the V4 site. Bottom: Receptive fields of the same neuronal site 125 and 14 randomly selected V1 neuronal sites used as predictors, constrained on sites that share at least 80% receptive field overlap with the V4 site. Right: EV fraction of V4 neural activity ( $n = 18$  site recordings per activity type) using 14 V1 predictor sites with less than 10% RF overlap (light green), 14 predictor sites with at least 80% RF overlap (green), and all predictors (dark green). Predictions were computed for recordings in response to the stimulus presentation (sliding bars and full-field checkerboard images) and gray screen presentation. **D.** Bottom and top left: Same as **F** but for monkey A sample V1 site 651. Right: Same as **C**, but for V1 ( $n = 378$  site recordings per activity type). Instead of 14, 10 prediction sites were used to predict V1 due to low sample count of V4 that fulfilled both types of RF overlap percentages. **E-F.** Same as **A-B** but for monkey L after subsampling sites to match the number of sites in monkey A ( $L_A$ ).

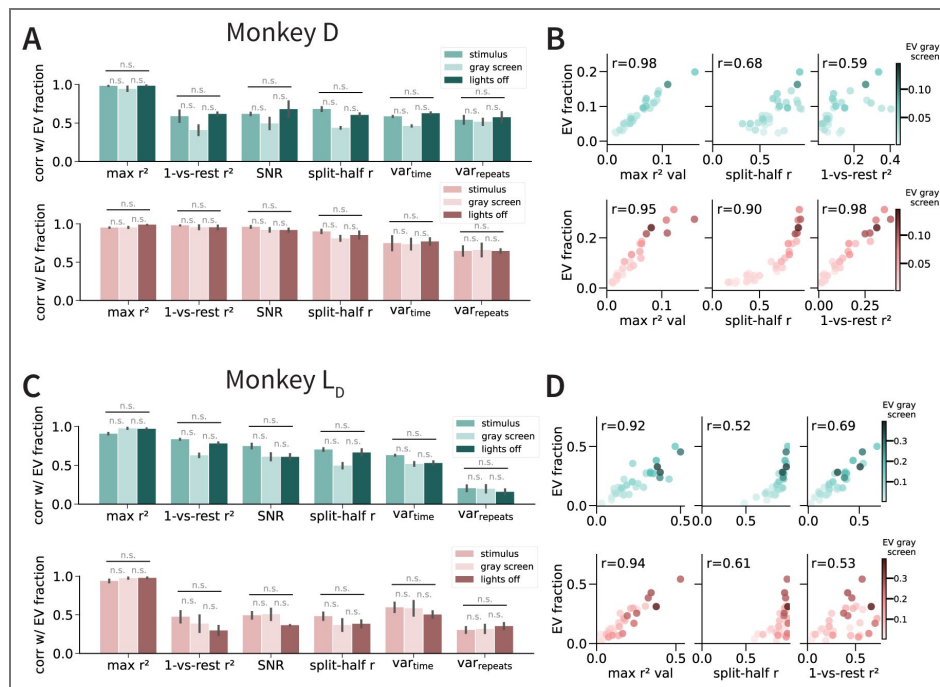


**Figure Supplement 9. Influence of SNR, variance, and split-half reliability is consistent across monkeys L and D.**

**A.** Correlation between different properties with the predictability of V4 (green) and V1 (coral) neuronal responses during the presence (dark color) or absence (light color) of visual stimulus in monkey D. **B.** Relationship between three properties and their predictability in sites for monkey D V4 (green) and V1 (coral) responses from stimuli presentations. Hue represents the degree of predictability for the same sites during gray screen presentations. **C–D.** Same as A–B but for subsample monkey L<sub>D</sub>.

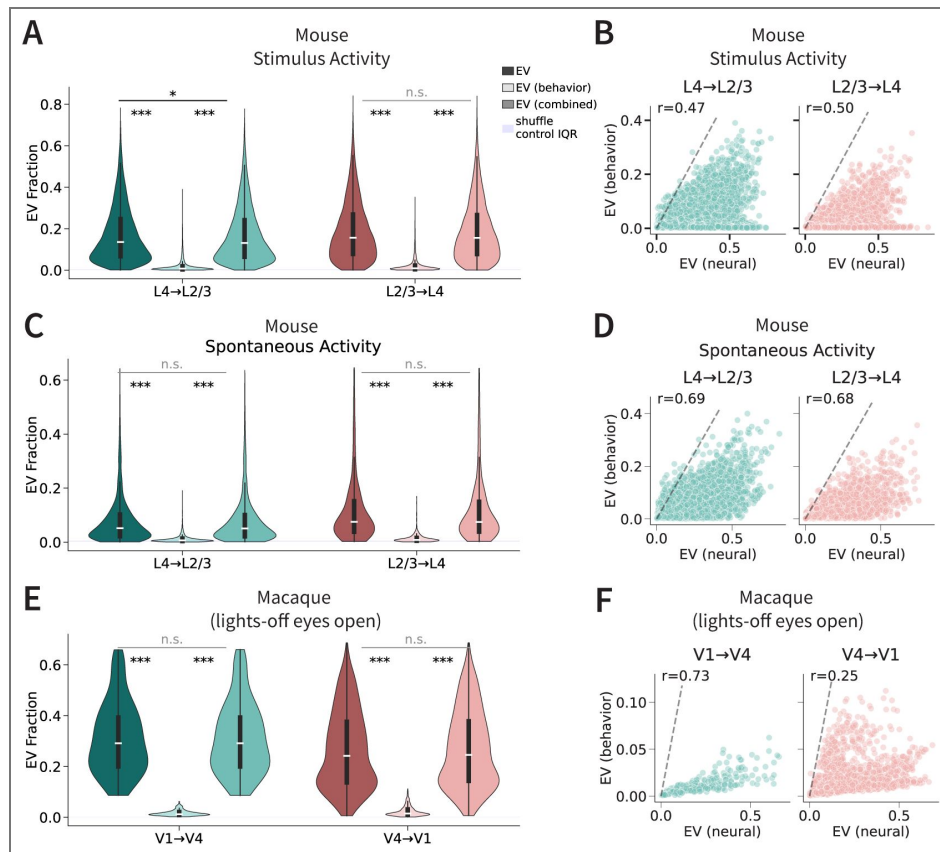


**Figure Supplement 10. Behavioral contributions to inter-areal predictability in mouse and monkey.**

A. Distribution of EV fraction for neural-only (dark colors), behavior-only (face-motion SVD and running speed; light colors), and combined mod-els (medium colors) in mouse L4 → L2/3 and L2/3 → L4 predictions during stimulus activity. B. Scatter plots comparing EV from behavior-only models (y-axis) versus neural-only models (x-axis) for mouse L2/3 response prediction (left) and mouse L4 response prediction (right). C–D. Same as A–B, but for spontaneous activity in mouse. E. Distribution of EV fraction for neural-only, pupil-only, and combined models in monkey L V1 → V4 and V4 → V1 predictions during resting state with eyes open. F. Scatter plots comparing EV from behavior-only models (y-axis) versus neural-only models (x-axis) for monkey V4 response prediction (left) and monkey V1 response prediction (right). The dashed line represents the line of equality ( $y=x$ ).

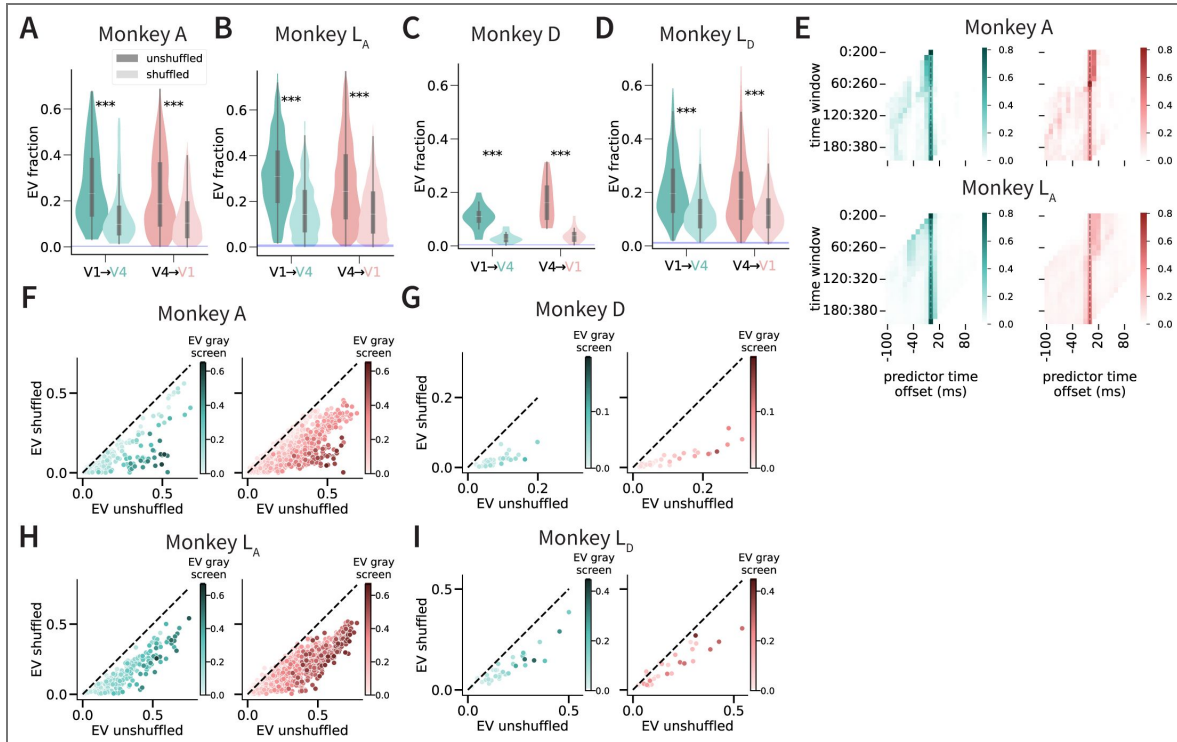


**Figure Supplement 11. Time-dependent effects on EV predictability in monkeys A and D.**

**A–D** Distribution of EV fraction in unshuffled (dark) and shuffled (light) trial-repeat activity in monkey A, monkey L subsampled to match the number of sites in monkey A ( $L_A$ ), monkey D, and monkey L subsampled to match the number of sites in monkey D ( $L_D$ ). \* denote paired permutation tests. **E.** Time offset prediction results across both V1 → V4 (left, green) and V4 → V1 (right, coral) prediction directions in monkeys A (top) and subsampled  $L_A$  (bottom). Each square corresponds to the fraction of neuronal sites whose neural activity was best predicted during that offset period and time window. **F–I.** Relationship between shuffled (y-axis) and unshuffled (x-axis) trial repeat EVs in V1 → V4 (left, green) and V4 → V1 (right, coral) directions in monkeys A, subsampled  $L_A$ , D, and subsampled  $L_D$ . Hue represents EV fraction during gray screen activity (see color scale on right).

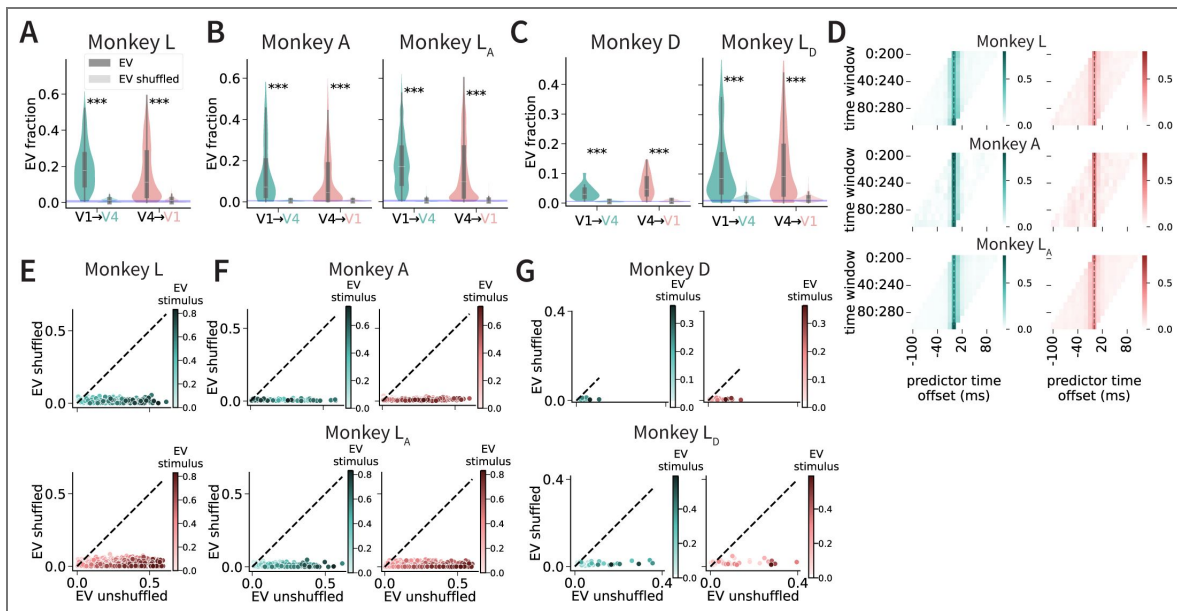


**Figure Supplement 12. Time-dependent effects on EV predictability during spontaneous conditions.**

Distribution of EV fraction for unshuffled (dark) and shuffled (light) trial-repeat activity during gray screen presentations (paired permutation test) in monkeys L, A, subsampled  $L_A$ , D, and subsampled  $L_D$ . \* denote paired permutation tests. **D.** Time offset prediction results across both  $V1 \rightarrow V4$  (left, green) and  $V4 \rightarrow V1$  (right, coral) prediction directions during gray screen presentations in monkeys A (top) and subsampled  $L_A$  (bottom). Each square corresponds to the fraction of neuronal sites whose neural activity was best predicted during that offset period and time window. **E-G.** Relationship between shuffled (y-axis) and unshuffled (x-axis) trial repeat EVs in  $V1 \rightarrow V4$  (left, green) and  $V4 \rightarrow V1$  (right, coral) directions in monkeys L (E), A & subsampled  $L_A$  (F), and D & subsampled  $L_D$  (G). Hue represents EV fraction during stimulus activity (see color scale on right).

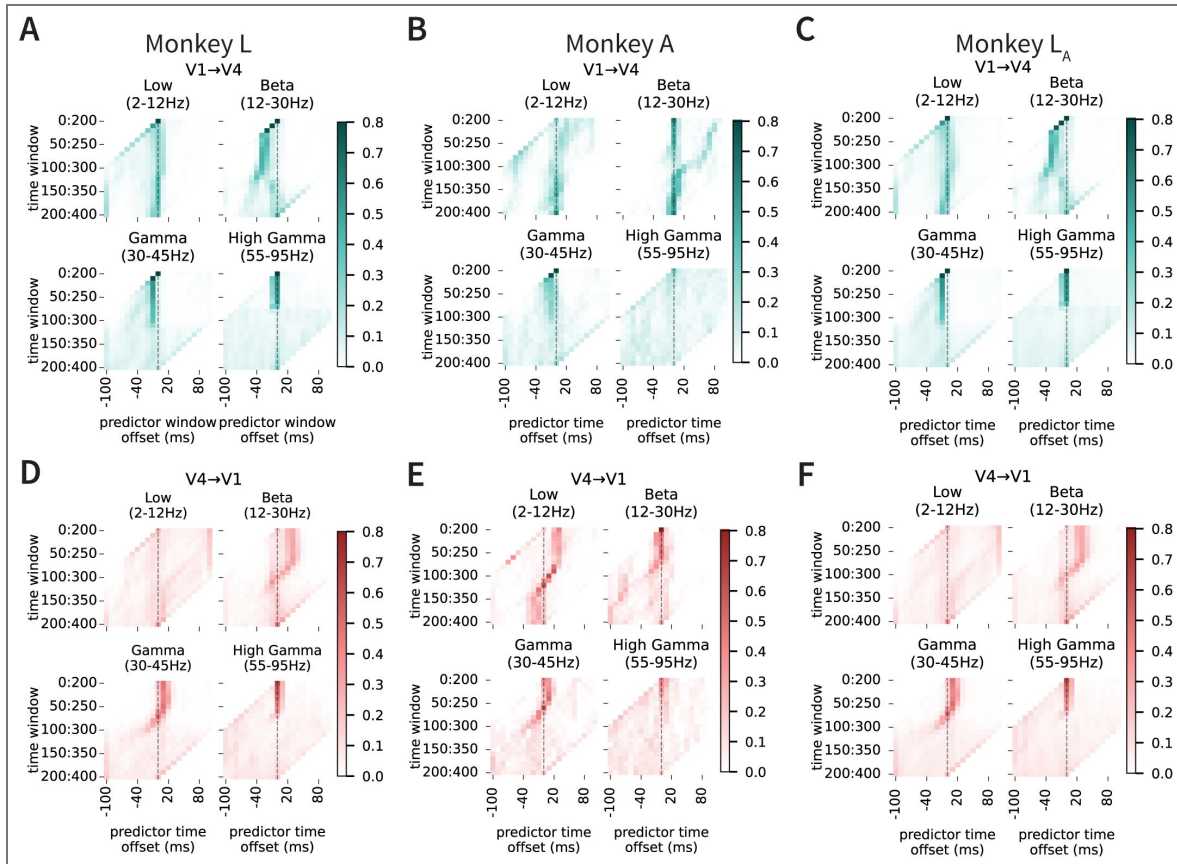


**Figure Supplement 13. Time-dependent effects on EV predictability across LFP bands in monkey V1/V4.**

**A-C.** Time offset prediction results across both V1 → V4 (left, green) and V4 → V1 (right, coral) prediction directions in monkeys L, A, and L<sub>A</sub>. Columns correspond to band-limited LFP amplitude (Hilbert envelope) from Low (2–12 Hz), Beta (12–30 Hz), Gamma (30–45 Hz), and High-gamma (55–95 Hz). LFP preprocessing included removal of narrow line artifacts (notch filter at 50 Hz and harmonics), band-pass filtering, and Hilbert amplitude extraction; envelopes were z-scored per unit. The dashed vertical line marks zero offset. **D-F.** Same as **A-B**, but predicting V1 from V4.

## Data availability

All the computational models and code for data analyses are publicly available at <https://github.com/4sdch/Trial-by-trial-inter-areal-interactions-in-visual-cortex>. All the data are publicly available (mice: [https://figshare.com/articles/dataset/Recordings\\_of\\_ten\\_thousand\\_neurons\\_in\\_visual\\_cortex\\_in\\_response\\_to\\_2\\_800\\_natural\\_images/6845348?file=12462734](https://figshare.com/articles/dataset/Recordings_of_ten_thousand_neurons_in_visual_cortex_in_response_to_2_800_natural_images/6845348?file=12462734), monkeys L and A: [https://gin.g-node.org/NIN/V1\\_V4\\_1024\\_electrode\\_resting\\_state\\_data](https://gin.g-node.org/NIN/V1_V4_1024_electrode_resting_state_data) and monkey D: <https://osf.io/9gz6f>).

## Acknowledgements

The authors would like to thank Elisa Pavarino, Leonardo Polina, Sara Djambazovksa, Jan Drugowitsch, Wei-Chung Allen Lee, Morgan Talbot, for providing comments on the manuscript.

## Additional information

### Funding

This work was supported by NIH grant R01EY026025 (GK) and NSF grant CCF-1231216 (GK). This work was partially supported by the European Union's Horizon 2020 research and innovation program under the Marie Skłodowska-Curie grant agreement No. 101007926, and RO1 award: NINDS R01 NS113890 to SS

### Funding

Funder	Grant reference number	Author
NIH	R01EY026025	Gabriel Kreiman
NSF	CCF-1231216	Gabriel Kreiman
NINDS	R01NS113890	Stelios Smirnakis

### Author ORCID iDs

**Dianna Hidalgo:** <https://orcid.org/0000-0001-8073-8432>

**Will Xiao:** <https://orcid.org/0000-0001-5555-3217>

**Carlos R Ponce:** <https://orcid.org/0000-0002-9887-3234>

**Stelios Smirnakis:** <https://orcid.org/0000-0002-1929-2811>

**Gabriel Kreiman:** <https://orcid.org/0000-0003-3505-8475>

## References

- Andermann ML**, Kerlin AM, Roumis DK, Glickfeld LL, Reid RC. (2011) Functional Specialization of Mouse Higher Visual Cortical Areas. *Neuron* **72**:1025-1039 <https://doi.org/10.1016/j.neuron.2011.11.013> | [PubMed](#)
- Avitan L**, Stringer C. (2022) Not so spontaneous: Multi-dimensional representations of behaviors and context in sensory areas. *Neuron* **110**:3064-3075 <https://doi.org/10.1016/j.neuron.2022.06.019> | [PubMed](#)
- Bastos AM**, Vezoli J, Bosman CA, Schoffelen JM, Oostenveld R, Dowdall JR, De Weerd P, Kennedy H, Fries P. (2015) Visual Areas Exert Feedforward and Feedback Influences through Distinct Frequency Channels. *Neuron* **85**:390-401 <https://doi.org/10.1016/j.neuron.2014.12.018> | [PubMed](#)
- Chacron MJ**, Longtin A, Maler L. (2003) The effects of spontaneous activity, background noise, and the stimulus ensemble on information transfer in neurons. *Network* **14**:803-824 [PubMed](#)
- Chen X**, Morales-Gregorio A, Sprenger J, Kleinjohann A, Sridhar S, van Albada SJ, Grün S, Roelfsema PR. (2022) 1024-channel electrophysiological recordings in macaque V1 and V4 during resting state. *Scientific Data* **9**:77 <https://doi.org/10.1038/s41597-022-01180-1> | [PubMed](#)

- Connor CE, Brincat SL, Pasupathy A. (2007) Transformation of shape information in the ventral pathway. *Current Opinion in Neurobiology* **17**:140-147 <https://doi.org/10.1016/j.conb.2007.03.002> | PubMed
- The MICrONS Consortium, Bae JA, Baptiste M, Bodor AL, Brittain D, Buchanan J, Bumbarger DJ, Castro MA, Celii B, Cobos E, *et al.* (2021) Functional connectomics spanning multiple areas of mouse visual cortex. *bioRxiv* <https://doi.org/10.1101/2021.07.28.454025>
- Dadarlat MC, Stryker MP. (2017) Locomotion Enhances Neural Encoding of Visual Stimuli in Mouse V1. *The Journal of Neuroscience: The Official Journal of the Society for Neuroscience* **37**:3764-3775 <https://doi.org/10.1523/JNEUROSCI.2728-16.2017> | PubMed
- Douglas RJ, Martin KAC. (2004) Neuronal circuits of the neocortex. *Annual Review of Neuroscience* **27**:419-451 <https://doi.org/10.1146/annurev.neuro.27.070203.144152> | PubMed
- Felleman DJ, Van Essen DC. (1991) Distributed hierarchical processing in the primate cerebral cortex. *Cerebral Cortex* **1**:1-47 <https://doi.org/10.1093/cercor/1.1.1-a> | PubMed
- Gazzaley A, Rissman J, Cooney J, Rutman A, Seibert T, Clapp W, D'Esposito M. (2007) Functional Interactions between Prefrontal and Visual Association Cortex Contribute to Top-Down Modulation of Visual Processing. *Cerebral Cortex* **17**:i125-i135 <https://doi.org/10.1093/cercor/bhm113> | PubMed
- Gilbert CD, Li W. (2013) Top-down influences on visual processing. *Nature Reviews Neuroscience* **14**:350-363 <https://doi.org/10.1038/nrn3476> | PubMed
- Gokcen E, Jasper AI, Semedo JD, Zandvakili A, Kohn A, Machens CK, Yu BM. (2022) Disentangling the flow of signals between populations of neurons. *Nature Computational Science* **2**:512-525 <https://doi.org/10.1038/s43588-022-00282-5> | PubMed
- Hartigan JA, Hartigan PM. (1985) The Dip Test of Unimodality. *The Annals of Statistics* **13**:70-84 <https://doi.org/10.1214/aos/1176346577>
- Hohaia W, Saurels BW, Johnston A, Yarrow K, Arnold DH. (2022) Occipital alpha-band brain waves when the eyes are closed are shaped by ongoing visual processes. *Scientific Reports* **12**:1194 <https://doi.org/10.1038/s41598-022-05289-6> | PubMed
- Hsu A, Borst A, Theunissen FE. (2004) Quantifying variability in neural responses and its application for the validation of model predictions. *Network: Computation in Neural Systems* **15**:91-109 [https://doi.org/10.1088/0954-898X\\_15\\_2\\_002](https://doi.org/10.1088/0954-898X_15_2_002) | PubMed
- Hubel DH, Wiesel TN. (1962) Receptive fields, binocular interaction and functional architecture in the cat's visual cortex. *The Journal of Physiology* **160**:106-154 <https://doi.org/10.1113/jphysiol.1962.sp006837> | PubMed
- Ibrahim LA, Schuman B, Bandler R, Rudy B, Fishell G. (2020) Mining the jewels of the cortex's crowning mystery. *Current Opinion in Neurobiology* **63**:154-161 <https://doi.org/10.1016/j.conb.2020.04.005> | PubMed
- Jiang X, Shen S, Cadwell CR, Berens P, Sinz F, Ecker AS, Patel S, Tolias AS. (2015) Principles of connectivity among morphologically defined cell types in adult neocortex. *Science* **350**:aac9462 <https://doi.org/10.1126/science.aac9462> | PubMed
- van Kerkoerle T, Self MW, Dagnino B, Gariel-Mathis MA, Poort J, van der Togt C, Roelfsema PR. (2014) Alpha and gamma oscillations characterize feedback and feedforward processing in monkey visual cortex. *Proceedings of the National Academy of Sciences* **111**:14332-14341 <https://doi.org/10.1073/pnas.1402773111> | PubMed
- Kreiman G. (2021) *Biological and Computer Vision* Cambridge: Cambridge University Press. <https://doi.org/10.1017/9781108649995>
- Lee WCA, Bonin V, Reed M, Graham BJ, Hood G, Glattfelder K, Reid RC. (2016) Anatomy and function of an excitatory network in the visual cortex. *Nature* **532**:370-374 <https://doi.org/10.1038/nature17192> | PubMed

- Markov NT, Ercsey-Ravasz MM, Ribeiro Gomes AR, Lamy C, Magrou L, Vezoli J, Misery P, Falchier A, Quilodran R, Gariel MA, *et al.* (2014) A weighted and directed interareal connectivity matrix for macaque cerebral cortex. *Cerebral Cortex* **24**:17-36 <https://doi.org/10.1093/cercor/bhs270> | PubMed
- Morales-Gregorio A, Kurth AC, Ito J, Kleinjohann A, Barthélemy FV, Brochier T, Grün S, van Albada SJ. (2024) Neural manifolds in V1 change with top-down signals from V4 targeting the foveal region. *Cell Reports* **43**:114371 <https://doi.org/10.1016/j.celrep.2024.114371> | PubMed
- Niell CM, Stryker MP. (2008) Highly Selective Receptive Fields in Mouse Visual Cortex. *The Journal of Neuroscience* **28**:7520 <https://doi.org/10.1523/JNEUROSCI.0623-08.2008> | PubMed
- Niell CM, Stryker MP. (2010) Modulation of visual responses by behavioral state in mouse visual cortex. *Neuron* **65**:472-479 <https://doi.org/10.1016/j.neuron.2010.01.033> | PubMed
- Okazaki Y, Abrahamyan A, Stevens CJ, Ioannides AA. (2008) The timing of face selectivity and attentional modulation in visual processing. *Neuroscience* **152**:1130-1144 <https://doi.org/10.1016/j.neuroscience.2008.01.056> | PubMed
- Papadopouli M, Smyrnakis I, Koniotakis E, Savaglio MA, Brozi C, Psilou E, Palagina G, Smirnakis SM. (2024) Brain orchestra under spontaneous conditions: Identifying communication modules from the functional architecture of area V1. *bioRxiv* <https://doi.org/10.1101/2024.02.29.582364>
- Park J, Papoutsi A, Ash RT, Marin MA, Poirazi P, Smirnakis SM. (2019) Contribution of apical and basal dendrites to orientation encoding in mouse V1 L2/3 pyramidal neurons. *Nature Communications* **10**:5372 <https://doi.org/10.1038/s41467-019-13029-0> | PubMed
- Pasupathy A, Popovkina DV, Kim T. (2020) Visual Functions of Primate Area V4. *Annual Review of Vision Science* **6**:363-385 <https://doi.org/10.1146/annurev-vision-030320-041306> | PubMed
- Petousakis KE, Park J, Papoutsi A, Smirnakis S, Poirazi P. (2023) Modeling apical and basal tree contribution to orientation selectivity in a mouse primary visual cortex layer 2/3 pyramidal cell. *eLife* **12**:e91627 <https://doi.org/10.7554/eLife.91627> | PubMed
- Polack PO, Friedman J, Golshani P. (2013) Cellular mechanisms of brain state-dependent gain modulation in visual cortex. *Nature Neuroscience* **16**:1331-1339 <https://doi.org/10.1038/nn.3464> | PubMed
- Reynolds JH, Chelazzi L. (2004) Attentional modulation of visual processing. *Annual Review of Neuroscience* **27**:611-647 <https://doi.org/10.1146/annurev.neuro.26.041002.131039> | PubMed
- Ringach DL (2009) Spontaneous and driven cortical activity: implications for computation. *Current Opinion in Neurobiology* **19**:439-444 <https://doi.org/10.1016/j.conb.2009.07.005> | PubMed
- Salinas E, Sejnowski TJ. (2001) Correlated neuronal activity and the flow of neural information. *Nature Reviews Neuroscience* **2**:539-550 <https://doi.org/10.1038/35086012> | PubMed
- Schmolesky MT, Wang Y, Hanes DP, Thompson KG, Leutgeb S, Schall JD, Leventhal AG. (1998) Signal Timing Across the Macaque Visual System. *Journal of Neurophysiology* **79**:3272-3278 <https://doi.org/10.1152/jn.1998.79.6.3272> | PubMed
- Schuman B, Dellal S, Prönneke A, Machold R, Rudy B. (2021) Neocortical Layer 1: An Elegant Solution to Top-Down and Bottom-Up Integration. *Annual Review of Neuroscience* **44**:221-252 <https://doi.org/10.1146/annurev-neuro-100520-012117> | PubMed
- Semedo JD, Jasper AI, Zandvakili A, Krishna A, Aschner A, Machens CK, Kohn A, Yu BM. (2022) Feedforward and feed-back interactions between visual cortical areas use different population activity patterns. *Nature Communications* **13**:1099 <https://doi.org/10.1038/s41467022-28552-w>
- Semedo JD, Zandvakili A, Machens CK, Yu BM, Kohn A. (2019) Cortical Areas Interact through a Communication Subspace. *Neuron* **102**:249-259.e4. <https://doi.org/10.1016/j.neuron.2019.01.026> | PubMed
- Serre T, Oliva A, Poggio T. (2007) A feedforward architecture accounts for rapid categorization. *Proceedings of the National Academy of Sciences* **104**:6424-6429 <https://doi.org/10.1073/pnas.0700622104> | PubMed

- Serre T, Wolf L, Bileschi S, Riesenhuber M, Poggio T. (2007) Robust Object Recognition with Cortex-Like Mechanisms. *IEEE Transactions on Pattern Analysis and Machine Intelligence* **29**:411-426 <https://doi.org/10.1109/TPAMI.2007.56> | [PubMed](#)
- Shen S, Jiang X, Scala F, Fu J, Fahey P, Kobak D, Tan Z, Reimer J, Sinz F, Tolias AS. (2020) Distinct organization of two cortico-cortical feedback pathways. *bioRxiv* <https://doi.org/10.1101/2020.02.27.968792>
- Stringer C (2018) Recordings of ten thousand neurons in visual cortex during spontaneous behaviors. figshare. <https://doi.org/10.25378/janelia.6163622>
- Stringer C, Michaelos M, Tsybouski D, Lindo SE, Pachitariu M. (2021) High-precision coding in visual cortex. *Cell* **184**:2767-2778.e15. <https://doi.org/10.1016/j.cell.2021.03.042> | [PubMed](#)
- Stringer C, Pachitariu M, Steinmetz N, Carandini M, Harris KD. (2019) High-dimensional geometry of population responses in visual cortex. *Nature* **571**:361-365 <https://doi.org/10.1038/s41586-019-1346-5> | [PubMed](#)
- Stringer C, Pachitariu M, Steinmetz N, Reddy CB, Carandini M, Harris KD. (2019) Spontaneous behaviors drive multidimensional, brainwide activity. *Science* **364**:eaav7893 <https://doi.org/10.1126/science.aav7893> | [PubMed](#)
- Talluri BC, Kang I, Lazere A, Quinn KR, Kaliss N, Yates JL, Butts DA, Nienborg H. (2023) Activity in primate visual cortex is minimally driven by spontaneous movements. *Nature Neuroscience* **26**:1953-1959 <https://doi.org/10.1038/s41593-023-01459-5> | [PubMed](#)
- Tang Y, Gervais C, Moffitt R, Nareddula S, Zimmermann M, Nadew YY, Quinn CJ, Saldarriaga V, Edens P, Chubykin AA. (2023) Visual experience induces 4–8 Hz synchrony between V1 and higher-order visual areas. *Cell Reports* **42**:113482 <https://doi.org/10.1016/j.celrep.2023.113482> | [PubMed](#)
- Wang Q, Burkhalter A. (2007) Area map of mouse visual cortex. *Journal of Comparative Neurology* **502**:339-357 <https://doi.org/10.1002/cne.21286> | [PubMed](#)
- Wosniack ME, Kirchner JH, Chao LY, Zabouri N, Lohmann C, Gjorgjieva J. (2021) Adaptation of spontaneous activity in the developing visual cortex. *eLife* **10**:e61619 <https://doi.org/10.7554/eLife.61619> | [PubMed](#)
- Yamins DLK, Hong H, Cadieu CF, Solomon EA, Seibert D, DiCarlo JJ. (2014) Performance-optimized hierarchical models predict neural responses in higher visual cortex. *Proceedings of the National Academy of Sciences* **111**:8619-8624 <https://doi.org/10.1073/pnas.1403112111> | [PubMed](#)
- Ponce (2025) Hidalgo et al eLife Monkey D. Open Science Framework. ID 9gz6f <https://osf.io/9gz6f>
- Stringer (2019a) Mouse recordings. figshare. <https://doi.org/10.25378/janelia.6845348>
- Roelfsema (2022) Monkey recordings. G-Node. <https://doi.org/10.12751/g-node.i20kyh>

## Peer reviews

### Reviewer #1 (Public review):

Summary:

In this study, the authors evaluated inter-areal interactions in different types of neuronal recordings, timescales, and species". The method consists of computing the variance explained by a linear decoder that attempts to predict individual neural responses (firing rates) in one area based on neural responses in another area.

The authors apply the method to previously published calcium imaging data from layer 4 and layers 2/3 of 4 mice, and simultaneously recorded Utah array spiking data from areas V1 and V4 of 3 monkeys. They report distributions over "variance explained" numbers for several combinations: from mouse V1 L4 to mouse V1 L2/3, from L2/3 to L4, from monkey V1 to monkey V4, and from V4 to V1. For their monkey data, they also report the corresponding results for different temporal shifts. Overall, they find the expected results: responses in each

of the two neural populations are predictive of responses in the other, more so when the stimulus is not controlled than when it is, and with sometimes different results for different stimulus classes (e.g., gratings vs. natural images).

Strengths:

- (1) use of existing data
- (2) addresses an interesting question

Weaknesses:

The data and analysis results are presented in a way that invites direct comparison between mouse L4->L2/3 variance explained numbers, and monkey V1->V4 variance explained numbers. This comparison is highly problematic and can't be taken at face value as the authors themselves clearly acknowledge in the Discussion and reply to the reviews. The datasets simply differ in too many aspects. If the goal of the authors is not to compare, then the analyses should be presented separately, allowing for a more detailed analysis of each (also see below).

Understanding which patterns in the data are robust and which are idiosyncratic to individual animals/recordings is complicated by the fact that some figures appear to show a single mouse and some averages over all four mice with no indication over whether the results are consistent across mice. For the monkey results, all figures in the main text appear to only show a single monkey, with the other two monkey results in the SI. Again, it is not clearly presented and discussed which aspects of the results are robust, and which differ between monkeys.

Furthermore, there are literally dozens of statistical comparisons between various conditions and metrics in the main figures without them being sufficiently organized around robust new insights, that will likely replicate, and that can inform our understanding of the underlying processes, or constrain computational models.

<https://doi.org/10.7554/eLife.105119.2.sa3>

## Reviewer #2 (Public review):

Summary:

In this work the authors investigated the extent of shared variability in cortical population activity in the visual cortex in mice and macaques under conditions of spontaneous activity and visual stimulation. They argue that by studying the average response to repeated presentations of sensory stimuli, investigators are discounting the contribution of variable population responses that can have significant impact at the single trial level. They hypothesized that, because these fluctuations are to some degree shared across cortical populations depending on the sources of these fluctuations and the relative connectivity between cortical populations within a network, one should be able to predict the response in one cortical population given the response of another cortical population on a single trial, and the degree of predictability should vary with factors such as retinotopic overlap, visual stimulation, and the directionality of canonical cortical circuits.

To test this, the authors analyzed previously collected and publicly available datasets and data recorded themselves. These include calcium imaging of the primary visual cortex in mice and electrophysiology recordings in V1 and V4 of macaques under different conditions of visual stimulation. The strength of this data is that it includes simultaneous recordings of hundreds of neurons across cortical layers or areas and under different conditions of sensory stimulation and behavioral state. However, the weaknesses of calcium dynamics (which has

lower temporal resolution and misses some non-linear dynamics in cortical activity) and multi-unit envelope activity and LFPs (which reflects fluctuations in population activity rather than the variance in individual unit spike trains), underestimates the variability of individual neurons which may vary widely in their participation in shared sources of variance.

From their analysis, they found that there was significant predictability of activity between layer II/III and layer IV responses in mice and V1 and V4 activity in macaques, although the specific degree of predictability varied somewhat with the condition of the comparison and with differences in the quality of recordings between the datasets. The authors deployed a variety of analytic controls and explored a variety of comparisons that are both appropriate and convincing that there is a significant degree of predictability in population responses at the single trial level consistent with their hypothesis. This demonstrates that a significant fraction of cortical responses to stimuli are not due solely to the feedforward response to sensory input, and if we are to understand the computations that take place in cortex, we must also understand how sensory responses interact with other sources of activity in cortical networks. Overall, this work highlights that, beyond the traditionally studied average evoked responses considered in systems neuroscience, there is a significant contribution of shared variability in cortical populations that may contextualize sensory representations depending on a host of factors that may be independent from the sensory signals being studied.

#### Strengths:

This work considers a variety of conditions that may influence the relative predictability between cortical populations, including receptive field overlap, latency that may reflect feed-forward or feedback delays, and stimulus type and sensory condition. Their analytic approach is well designed and statistically rigorous. They acknowledge the limitations of the data and do not over-interpret their findings.

#### Weaknesses:

The different recording modalities between species and scales (within vs. across cortical areas) limit the interpretability of the inter-species comparisons, and while this is not the stated goal of the authors, the juxtaposition of these two datasets invites comparison.

<https://doi.org/10.7554/eLife.105119.2.sa2>

### Reviewer #3 (Public review):

Neural activity in visual cortex has primarily been studied in terms of responses to external visual stimuli. While the variability of neural inputs to a visual area are known to also influence visual responses, the contribution of this stimulus independent component to overall visual responses has not been well characterized.

In this study, the authors analyze datasets from both mice (a previous V1 Ca<sup>++</sup> imaging study) and monkeys (data from a previous study and new large-scale electrophysiological recordings from V1-V4). Using regression models, they examine the predictability of neural activity between Layer 4 and Layer 2/3 in mice and between V1 and V4 in monkeys. Their main finding is that significant predictions are possible even in the absence of visual input, highlighting the influence of stimulus independent downstream activity on neural responses. These findings can inform future modeling work of neural responses in visual cortex to account for such non-visual influences.

The authors perform a thorough analysis comparing regression-based predictions for a wide variety of combinations of stimulus conditions and directions of influence. While many of the

predictability patterns are largely in line with expectations (eg., downstream layers/areas predicting upstream activity), it is valuable to have these relationships quantified as the authors have done here. Predictability also depended on stimulus type, but these dependencies were not consistent across animals, making it difficult to draw general conclusions. Finally, they show robust predictions even during spontaneous activity which are only partially accounted for by available behavioral metrics. Together, these analyses provide a valuable quantification of stimulus-independent components of visual cortical activity and their potential role in shaping sensory responses.

<https://doi.org/10.7554/eLife.105119.2.sa1>

## Author response:

The following is the authors' response to the original reviews

### Reviewer #1 (Public review):

We truly appreciate all the effort that the reviewer put into reading and understanding our work. With a total of 37 excellent questions, this is one of the most thorough reviews that we have received in a long time.

#### R1.0: Summary:

*In this study, the authors propose a "unifying method to evaluate inter-areal interactions in different types of neuronal recordings, timescales, and species". The method consists of computing the variance explained by a linear decoder that attempts to predict individual neural responses (firing rates) in one area based on neural responses in another area.*

*The authors apply the method to previously published calcium imaging data from layer 4 and layers 2/3 of 4 mice over 7 days, and simultaneously recorded Utah array spiking data from areas V1 and V4 of 1 monkey over 5 days of recording. They report distributions over "variance explained" numbers for several combinations: from mouse V1 L4 to mouse V1 L2/3, from L2/3 to L4, from monkey V1 to monkey V4, and from V4 to V1. For their monkey data, they also report the corresponding results for different temporal shifts. Overall, they find the expected results: responses in each of the two neural populations are predictive of responses in the other, more so when the stimulus is not controlled than when it is, and with sometimes different results for different stimulus classes (e.g., gratings vs. natural images).*

#### Strengths:

- (1) Use of existing data.
- (2) Addresses an interesting question.

*R1.1: Unfortunately, the method falls short of the state of the art: both generalized linear models (GLMs), which have been used in similar contexts for at least 20 years (see the many papers, both theoretical and applied to neural population data, by e.g. Simoncelli, Paninsky, Pillow, Schwartz, and many colleagues dating back to 2004), and the extension of Granger causality to point processes (e.g. Kim et al. PLoS CB 2011). Both approaches are substantially superior to what is proposed in the manuscript, since they enforce non-negativity for spike rates (the importance of which can be seen in Figure 2AB), and do not require unnecessary coarse-graining of the data by binning spikes (the 200 ms time bins are very long compared to the time scale on which communication between closely connected neuronal populations within an area, or between related areas, takes place).*

First, a few points of clarification.

(i) We worked with two-photon calcium imaging data (mice), and with the envelope of multi-unit activity (monkeys). While both of these types of signals are strongly correlated with spikes, neither of them can be truly considered to be a point process.

(ii) The reviewer points to Figure 2AB. The signals that we worked with can be negative. The black traces are the actual signals and show clear negative bouts, especially noticeable in the middle panel in Figure 2B. Of course, this does not mean that there are negative spike rates. This has to do with the way the data are normalized and not with the specific prediction method. However, the reviewer is correct in stating that the method that we used could also yield negative values even for non-negative spike rates.

(iii) We did not bin the macaque data into 200-ms time bins, but rather 25-ms time bins (line 548, Figure 1B legend). Additionally, we have now performed additional analyses with different window sizes, showing that the conclusions still hold (see Supplemental Figure 4 and lines 139-143).

To further address the reviewer's question, we implemented a Poisson GLM enforcing non-negativity on macaque MUAe data (without spontaneous activity subtraction, ensuring strictly positive values; lines 135-139, Supplemental Figure 1M). The model did not improve predictions over ridge regression, confirming our methodological choice. This method is not directly applicable to mouse calcium data, since the activity after baseline subtraction can be negative.

We did not use Granger or any other causality methods. The question of causality is certainly important, and there are multiple methods developed to assess causality in neural signals. We do not make any claims about causality in our study. A rigorous evaluation of causality is an interesting line of research for future work.

*R1.2: In terms of analysis results, the work in the manuscript presents some expected and some less expected results. However, because the monkey data are based on only one monkey (misleadingly, the manuscript consistently uses the plural 'monkeys'), none of the results specific to that monkey, nor the comparison of that one monkey to mice, are supported by robust data.*

We have now added data from 2 additional monkeys, including:

(i) A second monkey (monkey "A") from the same dataset (Chen et al., 2020), which includes all activity types except the lights off condition (lines 90-96, 120-132, 159, 161, 171, 183-185, 188-194, 200-203, 228-237, 254-258, 292-296, 334-342, 351-353, 358-364, 374-378, 387-393, 400-408, 414, 417-421, 539-540, 544-545, 680-681, 696-698; Supplemental figures 1-6, 8, 11, 12, and 13; Table 2).

(i) We collected new neural activity from one additional monkey (monkey "D") in collaboration with the Ponce lab (lines 90-96, 120-130, 132-134, 163-164, 228-235, 237-243, 292-296, 351-353, 374-378, 387-389, 539-540, 553-560, 696-698; Supplemental figures 1-2, 4, 6, 9, 11, and 12; Table 2). The new data include responses to the same checkerboard and gray screen images as the original dataset, along with responses during lights-off conditions.

*R1.3: One of the main results for mice (bimodality of explained variance values, mentioned in the abstract) does not appear to be quantified or supported by a statistical test.*

We have now formally quantified the bimodality of the relationship between one-vs-rest correlation and inter-laminar explained variance (EV) in mice using Hartigan's dip test, applied to neurons with  $EV > 0.4$ . The test confirmed significant bimodality in two of the three

mice (MP031 and MP032:  $p < 0.001$ ; MP033:  $p = 0.687$ ). These results are now included in the Results section (lines 307-311) and shown in Supplemental Figure 7A,D. In datasets that did not show bimodality by visual inspection (macaque recordings), the same test yielded non-significant results (e.g.,  $p = 0.994$ ), confirming that the statistical analysis distinguishes between bimodal and unimodal cases.

*R1.4: Moreover, the two data sets differ in too many aspects to allow for any conclusions about whether the comparisons reflect differences in species (mouse vs. monkey), anatomy (L2/3-L4 vs. V1-V4), or recording technique (calcium imaging vs. extracellular spiking).*

We also agree with this comment. Our goal is not to provide any direct quantitative comparison between the two species. We emphasize (lines 494-497) that the experiments in the two species differ along multiple dimensions, including: (i) differences in recording modalities (calcium vs. electrophysiology), (ii) associated differences in temporal resolution, neuronal types, and SNR, (iii) cortical targets (layers vs. areas), (iii) sample size, (iv) stimuli, (v) task conditions. In the revised manuscript, we also emphasized that the aim of this work is to investigate inter-areal interactions within each species rather than to draw quantitative comparisons between species (lines 497-499).

**Reviewer #1 (Recommendations for the authors):**

*R1.5 In the analysis of directionality, you stated that subsampling was done randomly. Presumably, there could be multiple subsamples that fulfill the control of split-trial  $r$ . Are you only showing results from one subsample or multiple subsamples?*

We show the median from 10 subsample permutations. This is now clarified in line 621.

*R1.6 About the measurement 1-vs-rest  $r^2$ . Understanding the definition is important for interpreting the results, but the definition was not clearly written. In lines 195-196, could you be more clear about whether the correlation is between the predicted neuron and other neurons in the predicted population or between the predicted neuron and the mean activity of the predictor population? Also, in line 212, why do you call this self-consistency? Isn't this a correlation between a neuron and the others?*

The 1-vs-rest  $r^2$  value, or self-consistency, is the correlation calculated for each neuron  $i$  and does not involve other neurons. Let  $\mathbf{r}_i^{(t)}$  indicate the response  $r$  of neuron  $i$  during trial  $t$  ( $t=1, \dots, T$  where  $T$  is the total number of trials). For a given trial  $t$ , we compute the average activity of the neuron excluding this trial:

$$\bar{\mathbf{r}}_i^{(rest)} = \frac{1}{T-1} \sum_{\substack{t=1 \\ t \neq t}}^T \mathbf{r}_i^{(t)}$$

Throughout, the superscript (*rest*) means “all repetitions excluding repeat  $t$ ”. The one-vs-rest correlation for the held-out repetition  $t$  is:

$$SC_i^{(t)} = \text{corr} \left( \mathbf{r}_i^{(t)}, \bar{\mathbf{r}}_i^{(rest)} \right)$$

We then average these correlations across all held-out repetitions:

$$\overline{SC}_t = \frac{1}{T} \sum_{t=1}^T SC_t^{(t)}$$

We now clarify this in the text (lines 304-306 and lines 642-647).

*R1.7 In Figure 6 G and I. The “all” condition contains more neurons than either of the other two. In this case, is this comparison fair or meaningful?*

The reviewer is also correct here. The comparisons between the  $<10\%$  and  $>80\%$  groups contain the same number of predictor neurons, and those are fair comparisons. The “all”

condition contains more predictor neurons, and, therefore, those comparisons are not fair. We clarified this point in lines 360-364.

We included the “all” condition here because we think that it is an instructive sanity check in terms of reporting how EV changes with more neurons, and also in terms of understanding why the EV values in the other two conditions are lower. Expanding on this point with a little bit of philosophy, ultimately, when considering a neuron in area B (e.g., V4) and the contributions from neurons in another area A (e.g., V1), one would like to have access to all the inputs (e.g., all the neurons in V1 that are monosynaptically connected to the target neuron in area V4). We do not have access to this type of information, and we do not make any claims about monosynaptic connectivity, let alone exhaustive sampling of inputs to a given neuron. The “all” condition merely provides a quantitative illustration of the fact that EV increases with the number of predictor neurons. This observation may be considered to be somewhat trivial, but it should be pointed out that the conclusion relies on the input neurons sharing information with the target neurons (e.g., perhaps one may not be able to predict V4 activity very well from the responses of millions of neurons in the cerebellum).

*R1.8 I believe the results section can be improved by adding some interpretation after each finding.*

We thank the reviewer for the suggestion. We generally like to separate results from interpretation. However, to honor the suggestion, we added brief interpretations throughout the results section (lines 142-143, 171-173, 272-273, 279-281, 331-333, and 361-364) and expanded on the interpretations in the Discussion section.

*R1.9 Line 52 - 74: It would be better to be more specific about what kind of neuronal interactions, e.g., noise correlation, synchrony, etc.*

We added a clarification on the types of interactions we study in lines 68-73.

*R1.10 Line 81. Something seems to be missing after "5500". 5500 trials? Neurons?*

We thank the reviewer for pointing this out. The number refers to neurons (fixed in line 87).

*R1.11 Line 94. The readers would appreciate more explanation of the method.*

We have expanded on the explanation, as suggested (lines 106-107).

*R1.12 Line 104. The fraction of visually responsive neurons seems to be small. Is this typically for mouse V1? Would this fraction be higher if you also used the peak, as you did for macaque data in your SNR calculation (line 412)? And what is this number for the recorded L4?*

The reviewer correctly points out the small number of visually responsive neurons.

We note that we now refer to the subset of neurons used for prediction analyses as visually reliable (VR) neurons (lines 115-116, 125-126, 178-179, 183-184, 211-212, 214-216, 217-226, 283-286), defined conservatively as neurons with SNR > 2 computed from the mean across all stimuli (not the peak to any one stimulus) and split-half reliability >0.8 (Methods, lines 569–590). This choice emphasizes neurons that are consistently informative over the full stimulus set.

Regarding the question of how typical the number of responsive neurons in mice is, the fraction of “responsive” neurons in mouse V1 varies widely depending on the definition and stimulus set but the fractions are substantially lower than those reported in monkeys (with different methods). For those of us more used to the macaque neurophysiology literature, this has been one of the biggest surprises coming from work in rodents. Many studies report a sizable group of non-responsive neurons in mouse V1 (e.g., as little as 37% percent of V1

neurons being responsive in at least 25% of the trials according to de Vries et al., Nat Neur, 2020). Our fraction of visually responsive neurons is small because it couples a conservative SNR metric with a high trial-reliability threshold.

As the reviewer notes, a peak-based metric based on any stimulus would be a less conservative criterion that would increase the fraction of neurons labeled responsive.

| R1.13 Line 113. Why not also give an exact percentage number?

We have given the exact percentage number (lines 125-126).

| R1.14 Line 128. Is this just because L2/3 has more neurons? If so, then isn't this trivial?

Our intention was to illustrate the best prediction performance we could get in either direction, which means including all L2/3 neurons. We have reworded our text to clarify (lines 149-151).

| R1.15 Line 134. Isn't this expected? Since V1 have more units than V4?

The reviewer is correct. As discussed in R1.7 in mice, we sought to report the best prediction performances in either direction. We have edited our text for clarity (lines 149-151).

| R1.16 Line 165-168. What's the logical connection between these two sentences? If the former is true, we should expect to see differences. Also, why the same population? Shouldn't you include non-visual neurons?

The two sentences in question are: "The difference in predictability in the absence of a stimulus could in principle change according to the directionality in inter-laminar interactions." and, "There was no statistically significant difference in the EV fraction between laminar directions (L4 → L2/3 vs. L2/3 → L4) using the same control population as in Figure 3B (Figure 5A-C and Figure Supplement 2H)." The key point here was to control for similar reliability values in order to make fair comparisons. We have added an additional comparison between directionalities focusing on nonvisual neurons (SNR < 2 & r < 0.8), and have also found no statistically significant difference between direction of predictability (Supplemental Figure 3A, right, lines 221-224).

| R1.17 Table 2. The information of which session corresponds to which experiment can be put in the table, which would be easier to read.

We have added which sessions correspond to which experiments in Table 2.

| R1.18 Figure 1, Captions for panel c and d. I don't see any colored arrows in the figure.

We removed the color descriptions (Figure 1C-D).

| R1.19 Figures 3, 4, and others. The annotations of "n.s." are very hard to see.

We changed the color so that it is easier to see now (Figures 3, 4, 6, and Supplementary Figures 1-4, 6, and 8-10).

| R1.20 Figure 5, panel A. The legend is too small.

We increased the legend size (Figure 5A).

| R1.21 Figure S5, panel D. Why are some of the data points connected?

The paired connections are illustrated specifically in the highly predictable neurons to highlight the two separate distributions of neurons. One group, the highly predictable and highly reliable group, maintains its inter-laminar predictability after projecting out the "non-visual" activity (lines 327-330), whereas the highly predictable yet unreliable group shows a

sharp decrease in inter-areal predictability, which corroborates the idea of non-visual components influencing neurons in mouse V1, as shown by Stringer et al. 2019b and consistent with our results.

*R1.22 l.91 "Ope" -> open?*

We fixed the typo (line 100).

*R1.23 Fig. 3C+D: Why is only one session used for this?*

One session was used to illustrate the distribution of split-half reliability values per area. Figure 3D contains information about all 5 stimulus sessions (see legend to Figure 3D).

*R1.24 "Even without controlling for the number of predictors or their respective split-half correlation values (627-688 sites in V1, 86-115 sites in V4), we found better predictability in the V1 to V4 direction than the reverse ( $p < 0.001$ , Figure Supplement 2I)." -> What does "even" mean here? Isn't this simply the null result if there is no true difference and the real reason the authors controlled for size?*

The reviewer's understanding is correct. We have edited our text for clarity (lines 157-160)

*R1.25 "We could predict V1 and V4 activity across all stimulus types ( $p < 0.001$ , paired permutation test of prediction vs. shuffled frames prediction)." -> better than chance? For all neurons on average? What does this mean? Isn't it trivial and 100% expected that neural activity in the visual cortex is above chance related to the visual input?*

We stated that sites in V1 and V4 could predict each other across all stimulus types before describing the differences between them. We agree that this observation is to be expected and indicated so now in the text (lines 185-186).

*R1.26 "The predictability was the highest in both directions for neuronal activity in response to a full field checkerboard images (Figure 4D). In the V1 → V4 direction, the EV fraction was higher when predicting a slow-moving small thin bar compared to a fast-moving large thick bar (Figure 4D, left), whereas the opposite was true for the V4 → V1 direction (Figure 4D, right)." -> What does this mean? Is this expected or not? Under what theories of cortical processing?*

The differences between EV prediction directions (V1 → V4: slow thin bars > fast thick bars; V4 → V1: fast thick bars > slow thin bars) could be because V4 responses are more reliable for the slow thin bars whereas V1 responses are more reliable for the fast thick bars (Supplemental Figure 5H–I). To account for this possibility, we controlled for differences in target-related properties by regressing out covariates like SNR, split-half correlation, and variance. In monkey L, regressing out reliability/drive within direction using these covariates, the V4 → V1 bar difference between slow thin bars and fast thick bars was not significant and the difference in the V1 → V4 difference direction was reduced (Supplemental Figure 5K, lines 198-203). This suggests that the asymmetry primarily reflects stimulus-dependent reliability of the *target* population rather than a strong directional selectivity.

To the best of our knowledge, there are no clear predictions that match these observations from existing theories of visual cortical processing, especially given the paucity of computational models that include stimulus velocity when describing the responses in area V4. There has been extensive work on theories of surround suppression, but it seems unlikely that the thick bars would elicit surround suppression given the size of the V4 receptive fields. Many current computational models that aim to fit the responses of neurons in the visual cortex use neural networks that take an image as visual input and yield activations. Most of these models do not incorporate stimulus movement, and even those that do incorporate

stimulus dynamics, only indirectly map onto interlaminar stimulus transformations or even between-area stimulus transformations. We hope that the results in this manuscript will help inspire and constrain better models of visual cortical processing.

*R1.27 Shouldn't all the predictability analysis be done conditioned on the stimulus in order to tell us more than the trivial "both V1 and V3, or L2/3 and L4, are driven by visual inputs"? (The spontaneous activity analyses are essentially that, for a small subset of the stimuli.)*

The key goal of this study is to quantify inter-areal interactions both under visual input and without visual input. This type of analysis is important because inter-areal interactions may depend both on visual inputs but also on neuronal inputs that are not triggered by visual signals. For example, extensive work in mice has now shown that neuronal responses in V1 depend on an animal's running speed, independently of any visual input. Even within the visual input conditions, we present analyses where we shuffle trial order (e.g., Figure 7, Supplementary Figure 11) to estimate the contribution of trial-by-trial variations that are independent of visual inputs and other analyses where we project out non-visual activity (e.g., Supplementary Figure 7).

*R1.28 "In visually responsive neurons, there was a significant reduction in EV during gray screen compared to visual stimulus presentation" -> perfectly expected. But the report-worthy result here is how much is left, not whether EV is decreased!*

We have changed the wording on the results to highlight the sustained predictability (lines 211-212). It is important to note that, although the reduction in EV during gray screen may be expected, this observation does *not* hold for all neurons. In fact, there are some neurons for which the EV during visual presentation is comparable to that during gray screen (Figure 5B,C,E: neurons that lie on the diagonal line).

*R1.29 "Similar to the conclusions drawn from the mouse data, the predictability of neuronal activity was higher in response to stimulus presentation than to gray screen presentations" -> Really? Conditioned on stimulus, or explainable by the well-known fact that both V1 and V4 are visually driven?*

As discussed in R1.28, in mice, there are many neurons where the EV during gray screen is comparable to that during stimulus presentation. In monkeys, most sites were visually driven. As the reviewer points out, we expected that EV during stimulus presentation would be higher than during gray screen; this observation is a reasonable sanity check. The difference between unshuffled trials and shuffled trials (Figure 7, Supplementary Figure 11) provides an estimate of the interactions that are not purely explained by visual inputs alone in monkeys.

*R1.30 "Unlike the mouse, macaque correlation of visual predictability between stimulus presentation and spontaneous activity was high across all types of spontaneous conditions" -> Why? Is this simply explainable by a lower mean response in the spontaneous condition in the mouse? Are these mouse and monkey experiments truly comparable? Isn't it surprising that spontaneous activity in the monkey visual cortex compared to evoked activity is higher than in the mouse?*

With respect to the question of whether spontaneous activity (or stimulus-evoked activity) in monkeys is higher than in the mouse, it is difficult to make these comparisons. We emphasize in the text the multiple differences between the experiments in both species. Our goal is *not* to perform any quantitative comparison across species (see R1.4). We changed the wording to remove any inference of comparison between species (lines 248-250).

*R1.31 Occasionally imprecise presentation. Ex "To further examine the non-stimulus driven component, we reasoned that if the shared information between areas were*

*strictly driven by the visual stimulus, then using the activity of a stimulus presentation repeat to one specific image could be used to predict the responses to any other stimulus repeat of the same image. On the other hand, if the shared activity does not have any stimulus-response information, then the prediction model would not work when considering responses across repeated presentations of identical stimuli in different trials. To test these two opposing ideas, we compared the inter-areal prediction EV fractions using unshuffled versus shuffled trials." -> Sets up two extreme strawmen (100% driven by stimulus vs 0% driven by stimulus). What does "model would not work" mean? EV=0? Hypotheses not ideas.*

Our intent was to set up two extreme hypotheses, not to claim that neurons must fall exclusively into one or the other. The two extremes help better interpret the results.

The reviewer indicates that these are straw-man hypotheses. This may well be the case. But note the responses to R1.12, R1.27, R1.28, and R1.29. The reviewer seems to assume that all or most neurons in the visual cortex should be mostly or exclusively driven by visual stimuli.

We also replaced “ideas” with “hypotheses”, as suggested. We have expanded the discussion of these points in the manuscript (lines 480-493). Many neurons occupy intermediate positions between these two extreme hypotheses. We clarified that “model would not work” refers to prediction accuracy approaching chance ( $EV \approx 0$ ).

*R1.32 "In both species and in both directions, inter-areal prediction EV fraction persisted ( $p < 0.001$ ," Doesn't persist mean EV is unchanged? But the test is  $EV > 0$  or not in both cases.*

We meant that EV values remained significantly above chance, not that they were unchanged. The statistical test was indeed whether  $EV > 0$  as the reviewer indicated. We have revised the text accordingly (lines 375-380).

*R1.33 "In mice, neurons showed a bimodal distribution in terms of their response predictability in shuffled and unshuffled trials" -> I don't see any bimodality in the figure, nor is there a statistical test provided for bimodality.*

In Figure 7C, a group of neurons lay essentially along the horizontal axis, whereas the other group is dispersed closer to the diagonal line. Specifically, the neurons that lay on the horizontal axis are also the ones whose responses are best predicted during gray screen activity. We have changed the text to clarify this point (lines 380-382).

*R1.34 "In the macaque V4 → V1 direction, there was a large proportion of neurons with peak EV when considering 25 ms to 50 ms offsets in the positive direction (i.e., V4 after V1, Figure 7I, right)." -> So what does this mean? Is this compatible with anything we know? This is the anti-causal direction so some kind of explanation would be warranted.*

In the V4 → V1 panel, a positive offset means we use V4 at  $t + \Delta t$  to predict V1 at  $t$  (and conversely in the V1 → V4 panel). Therefore, the fact that the peak EV occurs at +10–20 ms indicates that V1 leads V4 by ~10–20 ms: in other words, V1's earlier response best predicts V4's slightly later response. This observation is not anti-causal, but rather it is consistent with the canonical largely feed-forward V1 → V4 latency (e.g., Schmolesky et al., 1998 among many others). We clarified this in text (lines 400-404).

*R1.35 L. 307: "In monkeys," plural!?*

While this was not correct in the original version, we have now added data from two more monkeys.

*R1.36 L. 313: "we observed an approximately bimodal distribution of neuronal responses, with a large subset of neurons that do not show reliable responses to visual*

| *stimuli both in L4 and L2/3" -> where?*

The bimodal distribution can be appreciated in Figure 6B (1-vs-rest  $r^2$ , third panel, note neurons along the y-axis, see also R1.33) and Supplementary Figure 7B (lines 307-312). Additionally, as stated in R1.3, we have now formally quantified the bimodality of the relationship between one-vs-rest correlation and inter-laminar explained variance (EV) in mice using Hartigan's dip test (lines 310-313); see also Supplementary Figure 7A,D. In datasets that did not show bimodality by visual inspection (macaque recordings) the same test yielded non-significant results, confirming that the statistical analysis distinguishes between bimodal and unimodal cases.

| *R1.37 Random subsampling to control for population size done with how many subsamples? How are they combined? Variability across subsamples interpreted how?*

We performed 10 permutations and used the median distributions across permutations (line 621).

**Reviewer #2 (Public Review):**

R2.0: *"Summary:*

*In this work, the authors investigated the extent of shared variability in cortical population activity in the visual cortex in mice and macaques under conditions of spontaneous activity and visual stimulation. They argue that by studying the average response to repeated presentations of sensory stimuli, investigators are discounting the contribution of variable population responses that can have a significant impact at the single trial level. They hypothesized that, because these fluctuations are to some degree shared across cortical populations depending on the sources of these fluctuations and the relative connectivity between cortical populations within a network, one should be able to predict the response in one cortical population given the response of another cortical population on a single trial, and the degree of predictability should vary with factors such as retinotopic overlap, visual stimulation, and the directionality of canonical cortical circuits."*

*R2.1: To test this, the authors analyzed previously collected and publicly available datasets. These include calcium imaging of the primary visual cortex in mice and electrophysiology recordings in V1 and V4 of macaques under different conditions of visual stimulation. The strength of this data is that it includes simultaneous recordings of hundreds of neurons across cortical layers or areas. However, the weaknesses of calcium dynamics (which has lower temporal resolution and misses some non-linear dynamics in cortical activity) and multi-unit envelope activity (which reflects fluctuations in population activity rather than the variance in individual unit spike trains), underestimate the variability of individual neurons. The authors deploy a regression model that is appropriate for addressing their hypothesis, and their analytic approach appears rigorous and well-controlled.*

We agree with these points, and we discuss these specific limitations in capturing the variability of individual neurons in the Discussion section (lines 500-504). We have now also added analyses based on local field potentials (LFP). LFPs do not directly reflect the activity of individual neurons either.

| *R2.2: From their analysis, they found that there was significant predictability of activity between layer II/III and layer IV responses in mice and V1 and V4 activity in macaques, although the specific degree of predictability varied somewhat with the condition of the comparison with some minor differences between the datasets. The authors deployed a variety of analytic controls and explored a variety of comparisons that are both appropriate and convincing that there is a significant degree of predictability in*

*population responses at the single trial level consistent with their hypothesis. This demonstrates that a significant fraction of cortical responses to stimuli is not due solely to the feedforward response to sensory input, and if we are to understand the computations that take place in the cortex, we must also understand how sensory responses interact with other sources of activity in cortical networks. However, the source of these predictive signals and their impact on function is only explored in a limited fashion, largely due to limitations in the datasets. Overall, this work highlights that, beyond the traditionally studied average evoked responses considered in systems neuroscience, there is a significant contribution of shared variability in cortical populations that may contextualize sensory representations depending on a host of factors that may be independent of the sensory signals being studied.*

We agree that these datasets do not lend themselves well to directly separating and quantifying all the different sources of the predictive signals. We expand on this point in the Discussion section (lines 509-511).

*R2.3: The different recording modalities and comparisons (within vs. across cortical areas) limit the interpretability of the inter-species comparisons.*

We also agree with this comment. We emphasize that our goal is not to attempt a direct quantitative comparison across species (lines 497-499).

*R2.4: Strengths:*

*This work considers a variety of conditions that may influence the relative predictability between cortical populations, including receptive field overlap, latency that may reflect feed-forward or feedback delays, and stimulus type and sensory condition. Their analytic approach is well-designed and statistically rigorous. They acknowledge the limitations of the data and do not over-interpret their findings.*

*Weaknesses:*

*The different recording modalities and comparisons (within vs. across cortical areas) limit the interpretability of the inter-species comparisons. The mechanistic contribution of known sources or correlates of shared variability (eye movements, pupil fluctuations, locomotion, whisking behaviors) were not considered, and these could be driving or a reflection of much of the predictability observed and explain differences in spontaneous and visual activity predictions.*

We have expanded on the Discussion section to explicitly state the points raised by the reviewer (lines 494-509).

In mice, we have now also analyzed a separate dataset in which behavioral measurements were available, including running speed and facial motion (FaceMap SVDs). We used these to build behavioral-only and combined models to predict neural activity. We found that behavioral variables explained a modest but consistent portion of the variance across both spontaneous and stimulus conditions (Supplementary Figure 10A,C, lines 268-273).

For the macaque data, we analyzed pupil size as the only available behavioral measure in the macaque dataset. We focused specifically on the “resting state, eyes open” condition, where both neural activity and pupil measurements were available. Using ridge regression, we assessed the extent to which pupil size predicted neural activity in V1 and V4. Pupil size alone explained only a small fraction of the variance (Supplementary Figure 10E, lines 274-276).

*R2.5: Previous work has explored correlations in activity between areas on various timescales, but this work only considered a narrow scope of timescales.*

Without going into specifics about the numbers, it is hard to fully address this question. As the reviewer noted in R2.1, the mouse data analyzed here do not lend themselves to evaluating predictability on scales of tens of milliseconds. In the macaque data, we have now conducted additional analyses where we binned the activity across a range of bin sizes (10 ms to 200 ms). The new analyses are shown in Supplementary Figure 4, and described in lines 140-143, 160-163.

*R2.6: The observation that there is some degree of predictability is not surprising, and it is unclear whether changes in observed predictability with analysis conditions are informative of a particular mechanism or just due to differences in the variance of activity under those conditions. Some of these issues could be addressed with further analysis, but some may be due to limitations in the experimental scope of the datasets and would require new experiments to resolve.*

First, we note that several of the analyses and comparisons are within conditions and not across conditions, where by “condition” we mean the presence or absence of a stimulus or different stimuli (e.g., Figures 3, 5, 6, 7, Supplementary Figures 3-4, 7-13).

Second, we note that our mouse preprocessing standardized responses by spontaneous mean and SD per neuron, controlling baseline scale across conditions (lines 535-538). Because of this standardization, spontaneous traces have unit scale (mean = 0, SD = 1).

To test whether differences in variance underlie our findings, we calculated the variance for both species. For mice, we computed variance across repeats (visual) and across timepoints (lines 286-291). For the macaque moving-bar sessions, we computed variance across the concatenated held-out samples pooling timepoints, repeats, and bar identities (lines 291-292).

The V4 population showed a higher overall variance distribution compared to the V1 population (Supplementary Figure 2I-J), and L2/3 variance was also overall higher than L4 (Supplementary Figure 2D-E). We also see a modest monotonic relationship between EV fraction and this variance (mouse visual: Spearman  $\rho = 0.43-0.52$ ,  $p < 0.001$ ; macaque stimulus responses:  $\rho = 0.50-0.56$ ,  $p < 0.001$ ; macaque gray-screen responses:  $\rho = 0.38$ ,  $p < 0.001$ , Figure 6A,D), indicating variance contributes to (but is not the primary driver of) EV prediction fraction. We then adjusted for variance by fitting, within each stimulus condition, a linear regression of EV on variance (excluding shuffled-control rows) and conducted all comparisons on the resulting residual EV values, thereby isolating effects not attributable to variance (see Supplementary Figure 3E-G, lines 165-171).

**Reviewer #2 (Recommendations for the authors):**

*R2.7 Overall I found this manuscript to be very clearly written and the results compelling, although I found myself wanting a little more. I believe these datasets also include information about eye movements, pupil diameter, and maybe locomotion and whisking in the rodent work. I think it could be informative to ask the degree to which the predictability, particularly during the spontaneous activity, is attributable to these other known sources of variance in trial-by-trial measures. My concern is that during visual stimulation, the space of cortical responses is limited to a very narrow scope (observing a visual stimulus during fixation) whereas spontaneous activity includes a broader range of possibilities (different states of arousal, eye movement).*

We analyzed the role of behavioral variables that could explain the neural activity in mouse V1 (including the variables suggested by the reviewer, running speed, facemap SVDs). The open dataset authors warned not to use pupil size since in the dark, the measurements were not accurate. In terms of the contribution to the predictability of mouse V1 activity, these behavioral variables showed a weak yet significant contribution (Supplementary Figure 10A,C, lines 260-270).

*R2.8 By controlling for eye movements or pupil diameter during spontaneous measurements, would you improve your measure of predictability?*

When predicting neural activity in the lights-off eyes open condition, combining neural data of the predictor population with information of pupil size did not result in a statistically significant increase in EV fraction when predicting the target population (Supplementary Figure 10E, lines 276-278).

*R2.9 Also, there is work that shows feed-forward correlations between V1 and higher visual areas are observed in higher frequency activity, whereas feedback is associated with lower frequency activity. If you compared your predictability measure over bandpasses with different timescales, would you find the direction of V1-V4 interactions changes consistent with this previous work?*

To address this question, we extended our analyses to the local field potential signals (LFPs) in monkeys, using band-limited LFP power (2–12, 12–30, 30–45, 55–95 Hz). We reran the lag sweep analyses (10-ms steps; 200-ms windows slid every 10 ms) in both directions. The Gamma band showed a feed-forward signature in the early evoked period: the V1 → V4 predictability peaked at negative offsets (~10–30ms; V1 leads), and the V4 → V1 predictability peaked at positive offsets, consistent with previous findings. The results for low and beta frequency bands are also presented in the text (Supplemental Figure 13, lines 412-423).

**Reviewer #3 (Public review):**

*R3.0: Neural activity in the visual cortex has primarily been studied in terms of responses to external visual stimuli. While the noisiness of inputs to a visual area is known to also influence visual responses, the contribution of this noisy component to overall visual responses has not been well characterized.*

*In this study, the authors reanalyze two previously published datasets - a Ca<sup>++</sup> imaging study from mouse V1 and a large-scale electrophysiological study from monkey V1-V4. Using regression models, they examine how neural activity in one layer (in mice) or one cortical area (in monkeys) predicts activity in another layer or area. Their main finding is that significant predictions are possible even in the absence of visual input, highlighting the influence of non-stimulus-related downstream activity on neural responses. These findings can inform future modeling work of neural responses in the visual cortex to account for such non-visual influences.*

*R3.1: "A major weakness of the study is that the analysis includes data from only a single monkey. This makes it hard to interpret the data as the results could be due to experimental conditions specific to this monkey, such as the relative placement of electrode arrays in V1 and V4."*

We have now added the second monkey (monkey "A") from the same dataset (Chen et al., 2020), which includes all activity types except the lights-off condition. In addition, we collected new neural activity from one additional monkey (monkey "D") in collaboration with the Carlos Ponce lab (monkey A: seelines 90-96, 120-132, 159, 161, 171, 183-185, 188-194, 200-203, 228-237, 254-258, 292-296, 334-342, 351-353, 358-364, 374-378, 387-393, 400-408, 414, 417-421, 539-540, 544-545, 680-681, 696-698; Supplemental Figures 1-6, 8, 11, 12, and 13; monkey D: see lines 90-96, 120-130, 132-134, 163-164, 228-235, 237-243, 292-296, 351-353, 374-378, 387-389, 539-540, 553-560, 696-698; Supplemental Figures 1-2, 4, 6, 9, 11, and 12. The conclusions for the new monkeys are qualitatively similar to the ones reported previously. The main quantitative differences are due to the very large difference in the number of predictor sites (Table 2, lines 127-134).

*R3.2: The authors perform a thorough analysis comparing regression-based predictions for a wide variety of combinations of stimulus conditions and directions of influence. However, the comparison of stimulus types (Figure 4) raises a potential concern. It is not clear if the differences reported reflect an actual change in predictive influence across the two conditions or if they stem from fundamental differences in the responses of the predictor population, which could in turn affect the ability to measure predictive relationships. The authors do control for some potential confounds such as the number of neurons and self-consistency of the predictor population. However, the predictability seems to closely track the responsiveness of neurons to a particular stimulus. For instance, in the monkey data, the V1 neuronal population will likely be more responsive to checkerboards than to single bars. Moreover, neurons that don't have the bars in their RFs may remain largely silent. Could the difference in predictability be just due to this? Controlling for overall neuronal responsiveness across the two conditions would make this comparison more interpretable.*

First, we note that several of the analyses and comparisons are within conditions and not across conditions, where by “condition” we mean the presence or absence of a stimulus or different stimuli (e.g., Figures 3, 5, 6, 7, Supplementary Figures 3-4, 7-13).

In Figure 4, differences in target-population responsiveness could influence predictability across stimulus types, as the reviewer points out. We therefore controlled for this by modeling EV as a function of the following neuron properties: split-half  $r$ , SNR, one-vs-rest  $r^2$ , and response variance. Regression was performed within each direction, where we then used residuals for inference. When comparing residuals, the predictability of checkerboard responses remained statistically higher than the predictability of the responses to moving bars ( $p < 0.001$ , permutation test, Supplementary Figure 5K, lines 196-203), suggesting that the differences in predictability cannot be exclusively attributed to differences in the target population neuronal properties.

<https://doi.org/10.7554/eLife.105119.2.sa0>